



Cervenka Consulting Ltd.
Na Hřebenkách 55
150 00 Prague
Czech Republic
Phone: +420 220 610 018
E-mail: cervenka@cervenka.cz
Web: <http://www.cervenka.cz>

ATENA Program Documentation

Part 3-1

Example Manual

ATENA Engineering

Written by
Petr Kabele, Vladimír Červenka,
and **Jan Červenka**

Prague, March 2010



Trademarks:

ATENA is registered trademark of Vladimir Cervenka.

Microsoft and Microsoft Windows are registered trademarks of Microsoft Corporation.

Other names may be trademarks of their respective owners.

Copyright © 2000-2010 Cervenka Consulting Ltd.

CONTENTS

1	MATERIAL AND FRACTURE TESTS	1
1.1	Determination of tensile strength from a three point bending test (TPBB)	1
1.1.1	Introduction	1
1.1.2	Comments on FE model preparation	1
1.1.3	Results	3
1.1.4	References	3
1.2	Simulation of fracture energy measurement (GFM)	6
1.2.1	Introduction	6
1.2.2	Comments on FE model preparation	6
1.2.3	Results	7
1.2.4	References	7
1.3	Uniaxial compression test (UAC)	10
1.3.1	Introduction	10
1.3.2	Comments on FE model preparation	10
1.3.3	Results	11
1.3.4	References	11
1.4	Interface failure test (NGAP)	16
1.4.1	Introduction	16
1.4.2	Comments on FE model preparation	16
1.4.3	Results	16
1.5	Interface failure test (NGAP) 3D	21
2	STRUCTURAL ELEMENTS ANALYSES	24
2.1	Beam on elastic foundation (SPRI)	24
2.1.1	Introduction	24
2.1.2	Comments on FE model preparation	24
2.1.3	Results	25
2.2	Simulation of tension stiffening experiment (TST)	28
2.2.1	Introduction	28
2.2.2	Comments on FE model preparation	28
2.2.3	Results	29
2.2.4	References	29
2.3	Simulation of tension stiffening experiment (TST) 3D	34
2.3.1	Introduction	34
2.3.2	Comments on FE model preparation	34
2.4	Leonhardt's shear beam (LSB)	38
2.4.1	Introduction	38
2.4.2	Comments on FE model preparation	38
2.4.3	Results	39
2.4.4	References	39
2.5	Leonhardt's shear beam (LSB) 3D	43
2.6	Prestressed concrete beam (INTB)	46
2.6.1	Introduction	46
2.6.2	Comments on FE model preparation	46
2.6.3	Results	47
2.7	Prestressed concrete beam (INTB) 3D	51

2.8	Beam with external cables (EXTC)	52
2.8.1	Introduction	52
2.8.2	Comments on FE model preparation	52
2.8.3	Results	52
2.9	Beam with external cables (EXTC) 3D	56
2.10	Shear wall with opening (SWO)	57
2.10.1	Introduction	57
2.10.2	Comments on FE model preparation	57
2.10.3	Results	58
2.10.4	References	58
2.11	Punching failure of a slab (PUNC)	63
2.11.1	Introduction	63
2.11.2	Comments on FE model preparation	63
2.11.3	Results	64
2.11.4	References	64
2.12	Bond failure (BOND)	68
2.12.1	Introduction	68
2.12.2	Comments on FE model preparation	68
2.12.3	Results	70
2.12.4	References	71
2.13	Construction process of two-layer plate, 3D	78
2.13.1	Model description	78
2.13.2	Results – brick model	79
2.13.3	Results - shell model	80
3	MESH STUDY	82
3.1	Comparison of 2D, shell and 3D beam elements	82
3.1.1	Model description	82
3.1.2	Results	82
3.1.3	Conclusions	86

1 MATERIAL AND FRACTURE TESTS

1.1 Determination of tensile strength from a three point bending test (TPBB)

Keywords: plain concrete, softening, fracture localization, prescribed-force/prescribed-displacement boundary condition, Newton-Raphson method, rotating/fixed crack model

Input files: TPBB\TPBBF.cc2 (fixed crack)
TPBB\TPBBR.cc2 (rotated crack)

1.1.1 Introduction

Tensile strength of concrete may be indirectly determined from the result of a three point bending test on an unreinforced beam. The CEB-FIP MC90 model code [1] gives a formula, which relates the tensile strength to the measured flexural strength

$$f_{ct,fl} = f_{ctm} \frac{1 + \alpha_{fl} \left(\frac{h_b}{h_o} \right)^{0.7}}{\alpha_{fl} \left(\frac{h_b}{h_o} \right)^{0.7}} \quad (1.1)$$

Here

$f_{ct,fl}$	flexural strength (MPa)
f_{ctm}	tensile strength (MPa)
h_b	beam depth (mm)
h_o	100 (mm)
α_{fl}	coefficient, which depends on brittleness of concrete (value recommended by CEB-FIP MC90 is 1.5)

In this example, we verify validity of the above formula by simulating a three point bending experiment on a beam with known properties. The computed flexural strength is then compared to that obtained with Eq. (1.1).

1.1.2 Comments on FE model preparation

The analyzed beam geometry and support and loading conditions are shown in Figure 1-1. The input data for ATENA program are prepared through the ATENA 2-D graphical user interface (GUI) preprocessing window. Following are notes for each data block.

1.1.2.1 Materials

Concrete is modeled employing the ‘Sbeta Material’ model. Relevant material

properties used in the analysis are given in Table 1.1-1. The cubic compressive strength of 40 MPa is assumed, and the remaining parameters are left at their default values suggested by the ATENA program. The analysis is performed with both rotating and fixed crack model.

1.1.2.2 Topology

When specifying the problem topology, we place joints not only at the beam corners but also at the locations of supports and point loads to facilitate prescription of boundary conditions. The problem is modeled by a single macroelement, which is discretized by CCQ10SBeta type elements. To ensure good accuracy of the analysis, there should be at least 10 elements along the beam height. To this end, we specify element size 0.02 m.

1.1.2.3 Loads and supports and Solution parameters

Since the beam is unreinforced, we may expect that failure occurs at relatively low levels of load and reactions in supports. Thus, we may directly specify concentrated supports and loads, without a danger that these would cause local compressive crushing.

Our objective is to trace the load-displacement curve up to the post-failure softening regime. To this end, we may prescribe loading in terms of forces and use the arc-length method, which automatically changes the sign of load increment once a peak is attained. Alternatively, we may control displacement. Since displacement will keep on increasing even after the beam fails, we can employ either the Newton-Raphson method or the arc-length method. Due to its better stability, we opt for the Newton-Raphson solution method. (Note that, for large or brittle beams, a snap-back behavior may occur, in which case both displacement and force increments at the loading point change their sign upon failure. In such a situation, the arc-length solution is the only applicable method.)

To speed up convergence of the solution, we employ the full Newton-Raphson method, with tangent stiffness updated in each iteration. To automatically adjust the speed of analysis according to the nonlinearity of the response, we utilize the line search method. For this purpose we have to create a new set of ‘Solution Parameters’ (named N-R w/ LS), in which we set the appropriate options and parameters as summarized in Table 1.1-2.

1.1.2.4 Analysis steps

The load at which first cracking takes place can be estimated from the analytical elastic solution as 11.2 kN. Since the beam’s response up to this load is certainly elastic (and stable), we apply the first loading increment by prescribing force of 10 kN (load case LC2). In the following steps, we prescribe displacement increments at the loading point (load case LC3). The increment size is 0.01 mm. To accurately estimate the peak load (flexural strength), the increment size is further refined to 0.0025 mm around the peak.

1.1.2.5 Monitoring points

To facilitate the retrieval of load-displacement curves, we set up three monitoring points in the vicinity of the loading point. The first point monitors deflection, the second the applied force (associated with LC2) and the third the reaction

force at the load point (associated with LC3).

1.1.3 Results

The computed load-deflection curves obtained with the rotating and fixed crack model are shown in Figure 1-1. These data are retrieved by printing out the values at monitoring points. Note that the applied force monitored by point no. 2 changes only during the first step, when the loading is applied directly as the concentrated force. In the remaining steps, the loading is applied by prescribing displacement at the load-point, thus the additional loading force is obtained as the reaction in this point. The total applied load is then obtained as the sum of the force applied in step 1 and the reaction from the remaining steps.

Figure 1-2 shows, that the overall responses computed with the rotating and fixed crack models show almost no difference up to the tail of the post-peak part of the load-displacement curve. Crack patterns also slightly differ, especially in the final stage.

The flexural strength estimated by Eq. (1.1) with $\alpha_{fl}=1.5$ and $f_{ctm}=2.807$ MPa, is 3.959 MPa. The computed peak load is 15.180 kN with the rotating crack model and 14.951 kN with the fixed crack model, which corresponds to flexural strengths of 3.795 MPa and 3.738 MPa, respectively. The computed results differ from the estimated strengths by 4.1% and 5.6%, respectively.

$f_{ct,fl}$ from Eq. (1.1)	$f_{ct,fl}$ computed (rotating c.)	$f_{ct,fl}$ computed (fixed c.)
3.959 (MPa)	3.795 (MPa)	3.738 (MPa)

Closer inspection of the results by displaying cracks at individual steps of analysis in ATENA post-processing GUI also reveals that initially numerous vertical cracks form at the bottom of the beam. However, later cracking localizes and the beam fails by a single crack. Such a behavior is consistent with that observed in experiments.

1.1.4 References

- [1] FIB, Structural Concrete, Textbook on Behaviour, Design and Performance. Updated Knowledge of the CEB/FIB Model Code 1990, Vol. 1, FIB, 1999

Table 1.1-1 Material properties

Material type		SBETA material	
Elastic modulus	E_c	34.03	GPa
Poisson's ratio	ν	0.200	-
Compressive strength	f_c	34.000	MPa
Tensile strength	f_t	2.807	MPa
Type of tension softening		Exponential	
Fracture energy	G_f	70.18	N/m
Crack model		Fixed/Rotating	

Table 1.1-2 Solution parameters

Solution method	Newton-Raphson
Stiffness/update	Tangent/each iteration
Number of iterations	50
Error tolerance	0.010
Line search	on, with iterations

Table 1.1-3 Finite element mesh

Finite element type	Quadrilateral, CCQ10SBeta
Element shape smoothing	on
Optimization	Sloan

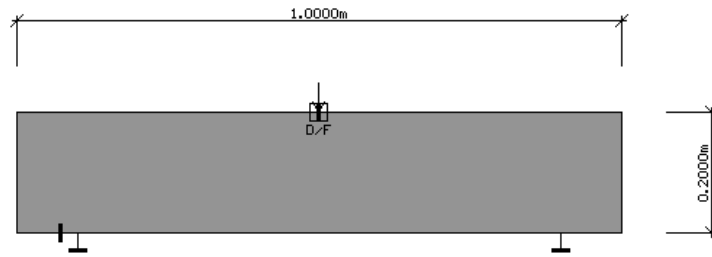


Figure 1-1: Geometry and boundary conditions of three-point bending beam

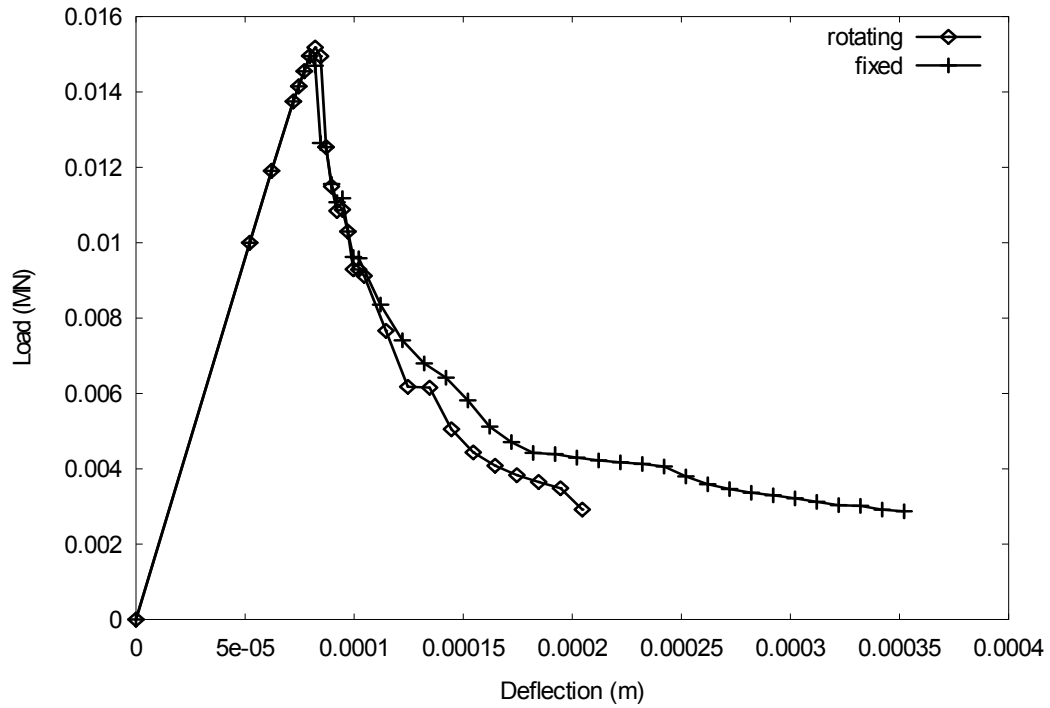


Figure 1-2: Computed load-displacement curve for a beam under three-point bending.

1.2 Simulation of fracture energy measurement (GFM)

Keywords: plain concrete, softening, prescribed-displacement boundary condition, Newton-Raphson method, mesh refinement

Input files: GFM\GFM1.cc2 (shorter notch)
GFM\GFM2.cc2 (longer notch)

1.2.1 Introduction

Fracture energy of a quasi-brittle material can be measured by conducting two fracture tests on double cantilever beam (DCB) specimens, with identical dimensions but slightly different initial notch lengths a_1 and a_2 . Fracture energy of the tested material is then obtained as the area enclosed by the two specimens' load-displacement curves, divided by the initial notch area difference $\Delta a.b$.

$$G_f = \frac{W_1 - W_2}{\Delta a.b} \quad (1.2)$$

In this example, we reproduce this measurement method by FE analyses. The measured fracture energy is compared with the fracture energy, which is input as a material parameter. The tested specimen dimensions and material properties are taken from Okada and Horii [1].

1.2.2 Comments on FE model preparation

1.2.2.1 Topology

The analyzed beam geometry and support and loading conditions are shown in Figure 1-3. The specimen thickness b_0 is 120 mm; however, to ensure a straight crack propagation, the specimen contains on both sides ten-millimeter-deep grooves along the symmetry plane. Consequently, the area weakened by the guides is represented by a separate macroelement with thickness $b=100$ mm. In order to achieve sufficient accuracy of the analysis, finite element mesh is refined around the expected crack path, so as to discretize the ligament by at least 20 elements.

Two specimens with different initial notch lengths $a_1=100$ mm and $a_2=105$ mm are analyzed. Thus the difference, Δa , is equal to 5 mm.

1.2.2.2 Materials

Concrete is modeled by the 'Sbeta Material' model. Relevant material properties used in the analysis are taken from Okada and Horii [1] and are listed in Table 1.2-1. The rotating crack model is used.

1.2.2.3 Loads and supports and Solution parameters

Since we need to trace the load-displacement curve up to the post-failure softening regime, we prescribe loading by controlling the displacements at the loading points and employ the Newton-Raphson solution method. The full Newton-Raphson method, with the tangent stiffness updated in each iteration, is used together with the line search technique. Relevant options and parameters as summarized in Table 1.2-2.

1.2.2.4 Analysis steps

Due to the presence of a notch, cracking starts at a very low load. Thus, a fine stepping has to be used from the very beginning of the analysis. The load-point displacement increment is kept constant, 0.003 mm.

1.2.3 Results

Figure 1-4 shows the load-displacement curves for the specimens with different initial notch lengths. The curves are numerically integrated to obtain the energies:

$$W_1 = 0.935 \text{ Nm (shorter notch } a_1)$$

$$W_2 = 0.873 \text{ Nm (longer notch } a_2)$$

With $\Delta a = 5 \text{ mm}$ and $b = 100 \text{ m}$, Eq. (1.2) yields the value of $G_f = 124.591 \text{ N/m}$. This value is only slightly higher than the inputted fracture energy (122 N/m), which proves validity of the measurement method. The slight overestimation results from the fact that cracking takes place not only on the main crack plane (as it is assumed in Eq. (1.2)), but some fine cracks also occur in directions almost perpendicular to the main crack.

G_f computed (N/m)	G_f input (N/m)
124.591	122

1.2.4 References

- [1] Okada T. and Horii, H., Effect of Specimen Size and Loading Rate on the Tension-Softening Curve Obtained by Back Analysis Method, in Fracture Mechanics of Concrete Structures – Proc. of FRAMCOS-3 (Reinhardt and Naaman eds.), AEDIFICATIO Publishers, 1998, pp. 89-100

Table 1.2-1 Material properties

Material type		SBETA material	
Elastic modulus	E_c	27.6	GPa
Poisson's ratio	ν	0.21	-
Compressive strength	f_c	26.4	MPa
Tensile strength	f_t	2.06	MPa
Type of tension softening		Exponential	
Fracture energy	G_f	122.0	N/m
Crack model		Rotating	

Table 1.2-2 Solution parameters

Solution method	Newton-Raphson
Stiffness/update	Tangent/each iteration
Number of iterations	50
Error tolerance	0.010
Line search	on, with iterations

Table 1.2-3 Finite element mesh

Finite element type	Quadrilateral, CCIsoQuad
Element shape smoothing	on
Optimization	Sloan

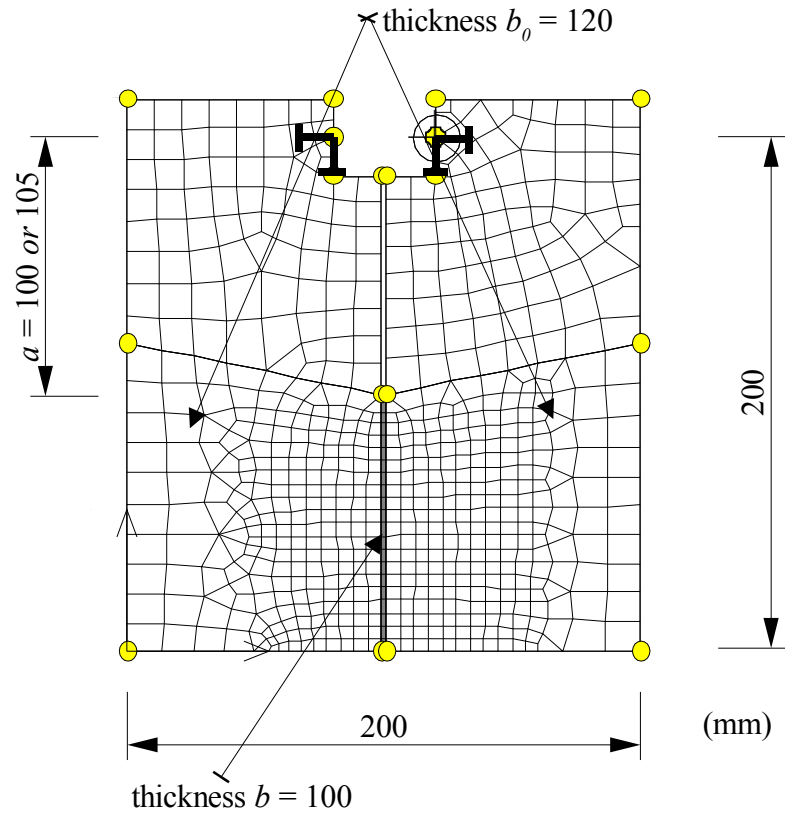


Figure 1-3: Configuration and FE mesh of the double cantilever beam specimen

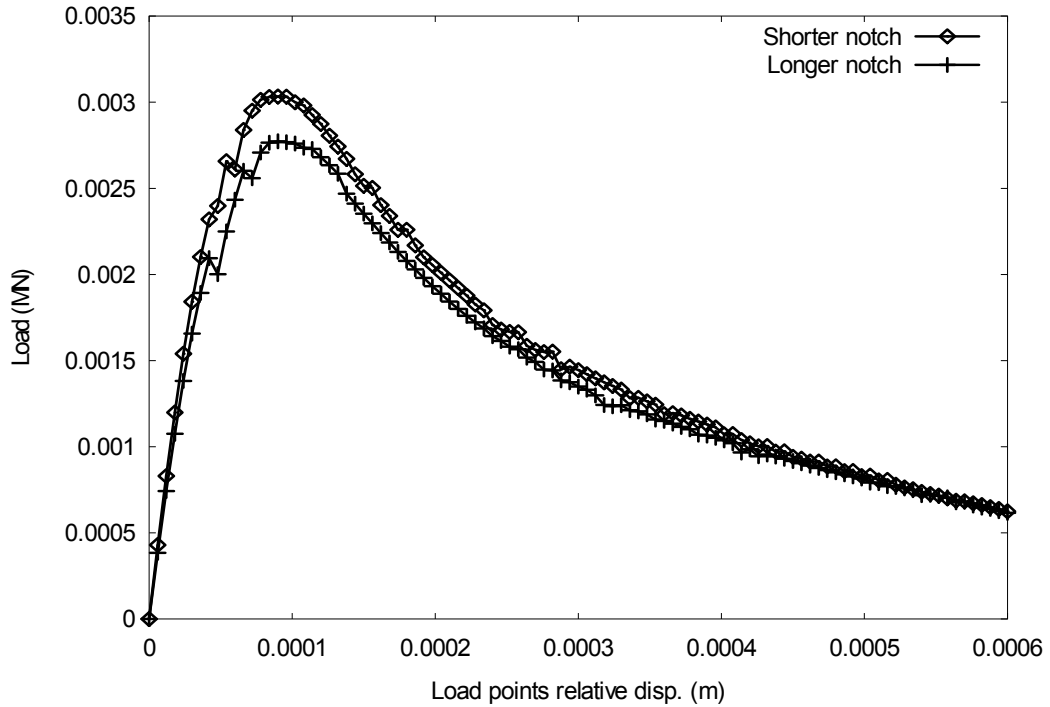


Figure 1-4: Load-displacement curves of DCB specimens

1.3 Uniaxial compression test (UAC)

Keywords: plain concrete, compressive softening, fracture localization, prescribed-displacement boundary condition, Newton-Raphson method

Input files: UAC\UAC050.cc2 (50 mm specimen)
 UAC\ UAC100.cc2 (100 mm specimen)
 UAC\ UAC200.cc2 (200 mm specimen)

1.3.1 Introduction

This example shows how ATENA treats compressive softening and the localization of fracture, which is associated with it.

Van Mier [1] conducted uniaxial compression tests on concrete prisms with identical cross-sections but various heights 50, 100 and 200 mm. The experiments indicated that all the specimens failed by formation of inclined planes of localized fracture. While in the 200 mm high prism, there was a large continuous failure plane, the 100 and 50 mm prisms showed several intersecting planes. However, the experiments revealed that the amount of energy required for fracturing a specimen was independent of its height (in a similar way as under uniaxial tension). Furthermore, the experiments showed that, if displacement corresponding to elastic deformation was subtracted from the post-peak part of each load-displacement curve, the resulting curves were almost identical for all three specimens.

ATENA allows treating these phenomena by directly inputting the compression softening stress-displacement relationship as a material property, in a similar manner as it is done for tension. Use of the concept is demonstrated by reproducing the van Mier's experiments in this example.

1.3.2 Comments on FE model preparation

1.3.2.1 Topology

We analyze three plain concrete specimens with heights 50, 100 and 200 mm and cross-section of 100x100 mm. Plane stress is assumed. An uniform mesh is used. The element size is 25 mm and is the same for all the specimens. To facilitate fracture localization, a band of material, which is slightly more brittle under compression, is inserted in each specimen (Figure 1-5). The height of this band may be arbitrary but should correspond to the height of a single element.

1.3.2.2 Materials

Concrete is modeled by the 'Nonlinear Cementitious' material model. Relevant material properties used in the analysis are listed in Table 1.3-1.

1.3.2.3 Loads and supports and Run

It is assumed that friction between loading plates and a concrete specimen is

perfectly removed. The bottom line of a specimen is fixed in vertical direction while the top line is loaded by prescribed uniform displacement. In addition, the bottom left corner is fixed horizontally. Since we control displacement, we may employ the Newton-Raphson solution method to trace the response up to the post-peak regime. Relevant options and parameters are summarized in Table 1.3-2.

1.3.3 Results

In all three specimens we can observe almost uniform deformation taking place up to the peak load. After the peak, the axial deformation localizes into the horizontal band of more brittle elements. The deformation of this band further induces lateral tension to the adjacent elements, causing their splitting in the direction parallel with the applied load. The failure pattern is documented in Figure 1-9 for the 200 mm specimen. This cracking behavior differs from that reported by van Mier [1], who observed formation of inclined failure planes. Nevertheless, graphs in Figure 1-6, Figure 1-7, and Figure 1-8 show, that the present approach successfully captures the overall stress-strain behavior for specimens of various heights.

1.3.4 References

- [1] Van Mier, J.G.M., Strain-softening of concrete under multiaxial loading conditions, Ph.D. Dissertation, Technical University of Eindhoven, 1984

Table 1.3-1 Material properties

Material type		Nonlinear cementitious	
Elastic modulus	E_c	38	GPa
Poisson's ratio	ν	0.2	-
Compressive strength	f_c	43.9	MPa
Tensile strength	f_t	2.987	MPa
Fracture energy	G_f	74.67	N/m
Plastic strain at strength f_c	ϵ_{cp}	9.4×10^{-4}	
Onset of non-lin. behavior in compression	f_{c0}	30	MPa
Critical compressive disp. (loc. band)	w_d	5×10^{-4}	m
Critical compressive disp. (rest of spec.)	w_d	6×10^{-4}	m

Table 1.3-2 Solution parameters

Solution method	Newton-Raphson	
Stiffness/update	Tangent/each iteration	
Number of iterations	50	
Error tolerance	0.001	
Line search	on, with iterations	

Table 1.3-3 Finite element mesh

Finite element type	Quadrilateral, CCIsoQuad	
Element shape smoothing	on	
Geometrical nonlinearity	on	
Optimization	Sloan	

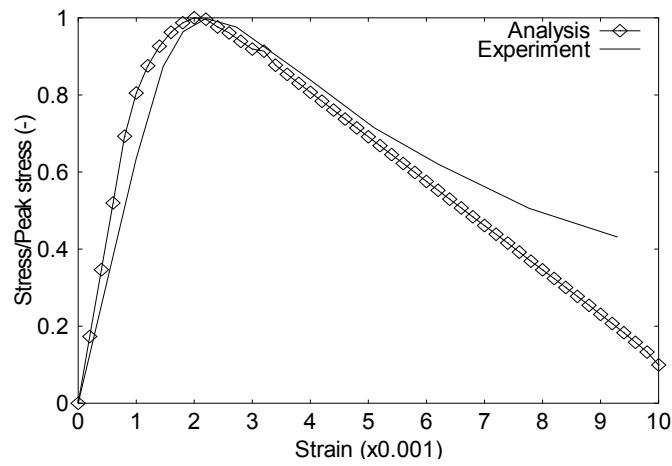


Figure 1-6: Overall stress-strain curves of 50 mm specimen

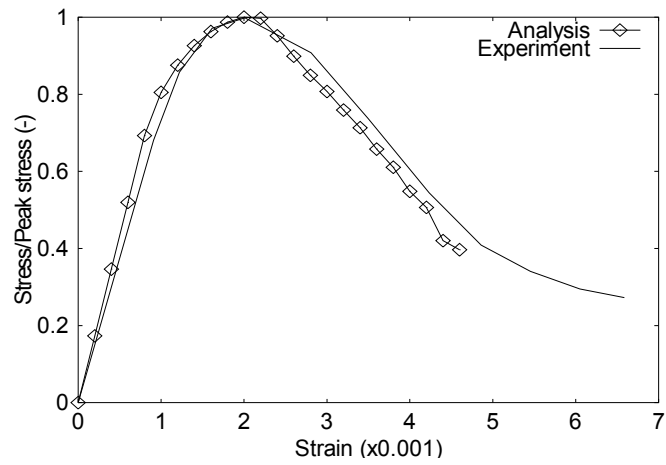


Figure 1-7: Overall stress-strain curves of 100 mm specimen

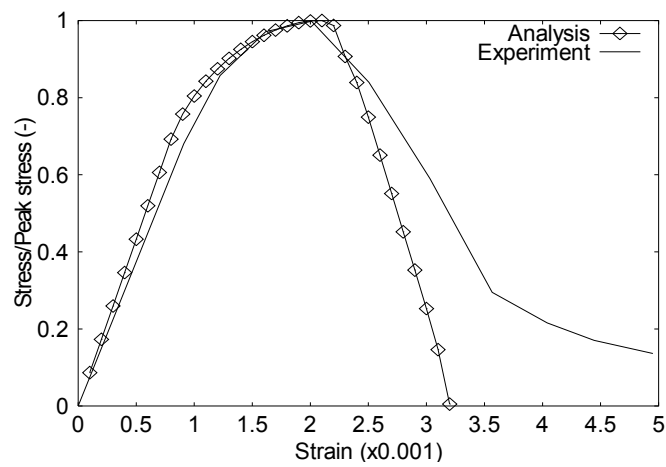


Figure 1-8: Overall stress-strain curves of 200 mm specimen

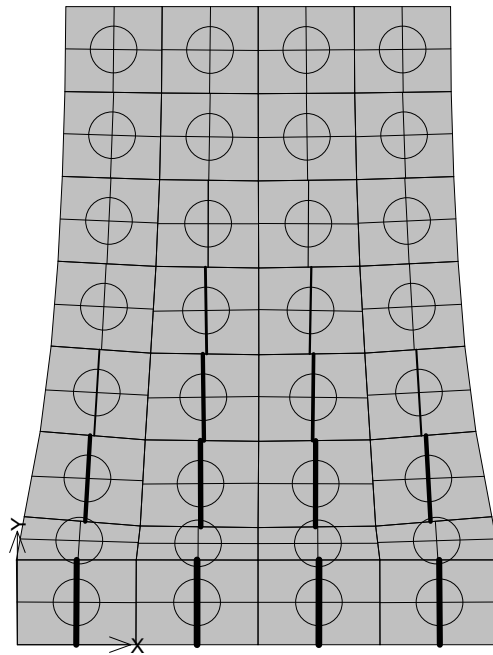


Figure 1-9: Computed crack pattern and deformed shape of the 200 mm specimen after the peak

1.4 Interface failure test (NGAP)

Keywords: concrete-concrete interface, contact

Input files: NGAP\NGAP.cc2

1.4.1 Introduction

This is a numerical experiment which demonstrates how ATENA handles phenomena associated with interfacial failure and slip. The analyzed specimen consists of two concrete slabs bonded by a weak interface (Figure 1-10). The bottom slab is fixed in both horizontal and vertical directions along its bottom face. A steel plate is attached to the top slab; a perfect bond is assumed between the plate and concrete. The specimen is first vertically compressed through the steel plate. Consequently, while keeping the loading plate's vertical displacement fixed, horizontal load is applied at its left edge. The load causes shearing of the specimen, which results in failure and slip along the concrete-concrete interface and cracking of the concrete slabs.

1.4.2 Comments on FE model preparation

1.4.2.1 Materials

Concrete of both slabs is modeled by the 'SBETA' material model, with parameters given in Table 1.4-1. Material of the steel plate is represented by the bilinear von Mises model (Table 1.4-2). In addition, we have to specify the concrete-concrete interface properties (2-d interface material model) – see Table 1.4-3.

1.4.2.2 Topology

The model consists of three macroelements representing the two concrete slabs and the steel plate. A rigid connection is specified for the line between the steel plate and the upper concrete slab. The connection between the two concrete macroelements is specified as interface, gap type. The previously defined interface material model is assigned to it.

1.4.2.3 Loads and supports and Run

The bottom face of the bottom concrete slab is fixed in both x and y directions (load case LC5 and LC6). Compression to the specimen is applied by prescribing the uniform vertical displacement of 0.07 mm at the top surface of the steel plate (LC2). The corresponding normal pressure is about 15.3 MPa and is almost uniform along the interface (Figure 1-10). In the consequent steps, the top surface is kept fixed in the vertical direction (LC3) while prescribing horizontal displacement to the left edge of the plate (LC4) - Figure 1-11. The horizontal loading is applied in 21 steps.

1.4.3 Results

As seen in Figure 1-12 and Figure 1-13, the overall response of the specimen is

dominated by the slip that occurs at the concrete-concrete interface, although some cracking of the concrete blocks takes place, too. Figure 1-10 and Figure 1-11 indicate that interfacial stresses remain almost uniform throughout the experiment. Given the normal compression of 15.3 MPa, the interfacial shear strength should be:

$$\tau_{\max} = c + \sigma_n \varphi = 1 + 0.1 \cdot 15.3 = 2.53 \text{ (MPa)}$$

Figure 1-11 shows that at the end of the experiment, the stress along the interface is approximately equal to this theoretical value.

Table 1.4-1 Material properties of concrete

Material type		SBETA material	
Elastic modulus	E_c	30.32	GPa
Poisson's ratio	ν	0.0	-
Compressive strength	f_c	25.5	MPa
Tensile strength	f_t	2.317	MPa
Type of tension softening		Exponential	
Fracture energy	G_f	111.5	N/m
Crack model		Fixed	

Table 1.4-2 Material properties of steel

Material type		Bilinear steel von Mises	
Elastic modulus	E_c	210	GPa
Poisson's ratio	ν	0.3	-
Yield strength		170	MPa
Hardening modulus		0	MPa

Table 1.4-3 Material properties of concrete-concrete interface

Material type		2D interface	
Normal stiffness	K_{nn}	3×10^6	MN/m^3
Tangential stiffness	K_{tt}	3×10^6	MN/m^3
Tensile strength	f_t	0	MPa
Cohesion	c	1	MPa
Friction coefficient	φ	0.1	-

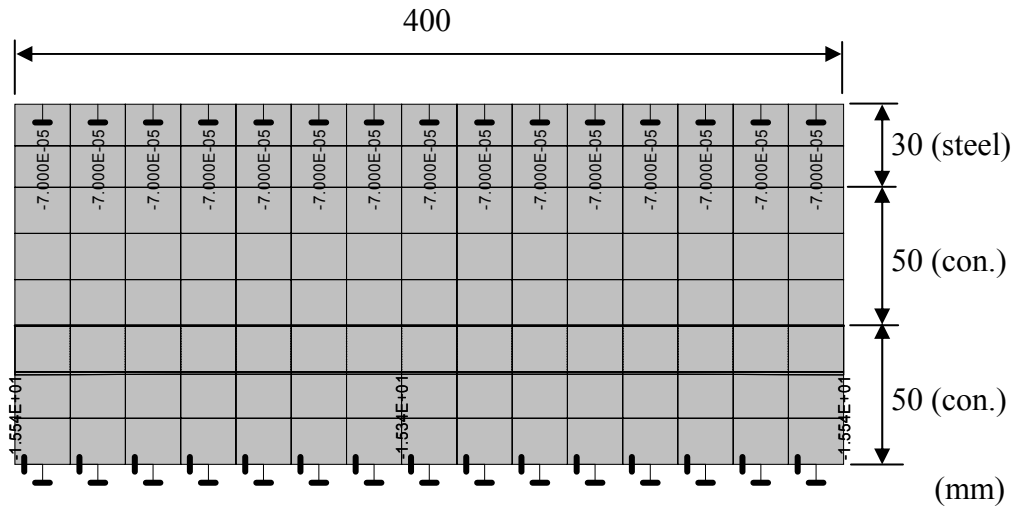


Figure 1-10: Dimensions of interface test specimen. Boundary conditions applied in the first load step and corresponding distribution of interfacial normal stress.

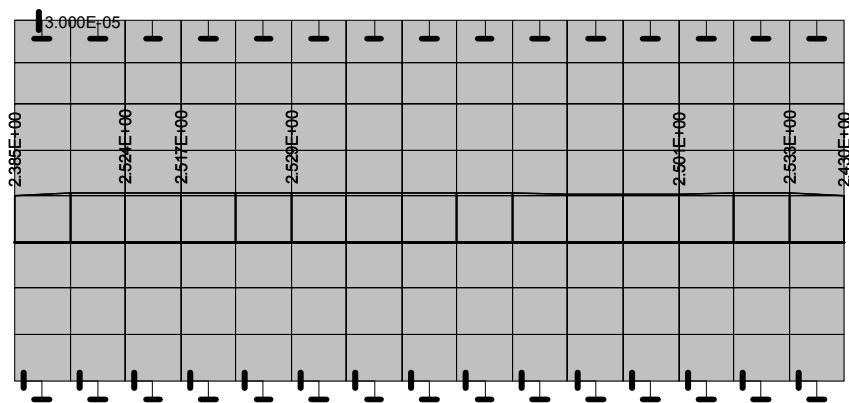


Figure 1-11: Boundary conditions applied in load steps 2 to 22. Distribution of interfacial shear stress after step 21.

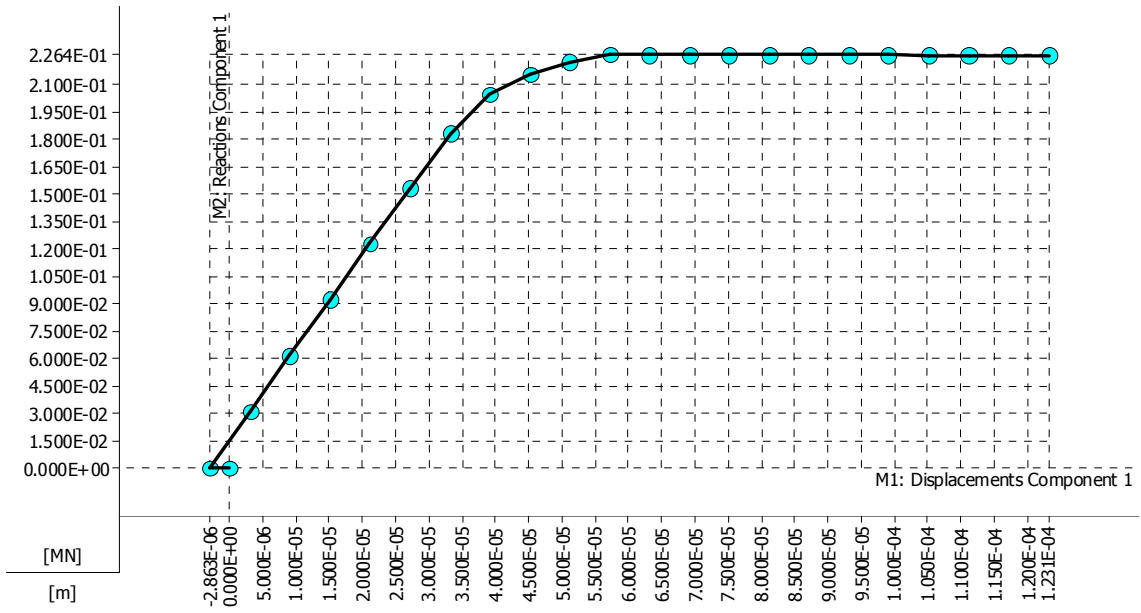


Figure 1-12: Computed horizontal load vs. load-point displacement relation

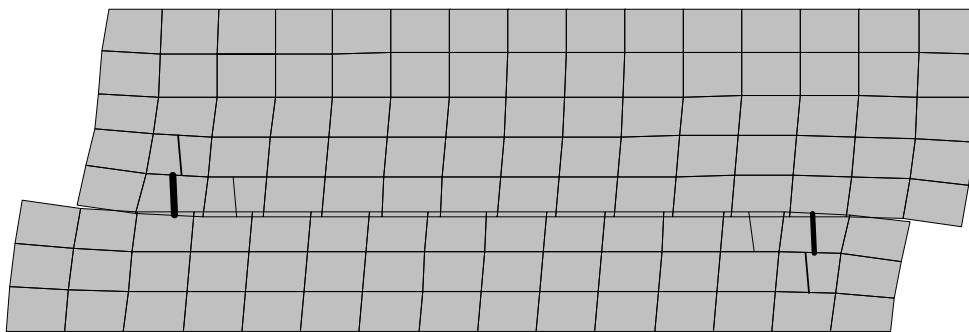


Figure 1-13: Cracking and deformed shape after load step 21

1.5 Interface failure test (NGAP) 3D

Input files: NGAP\NGAP.cc3

The 3D analysis is based on a model with the same dimensions and properties as in 2D. However, there are some differences. The horizontal load is applied as a point force in the center of the steel plate in form of prescribed displacement (shearing action). Only symmetrical half of the body is considered to reduce the size of numerical model (and to keep the model well supported). Material in this case is CC3DnonLinCementitious2 its parameters correspond with the 2D model.

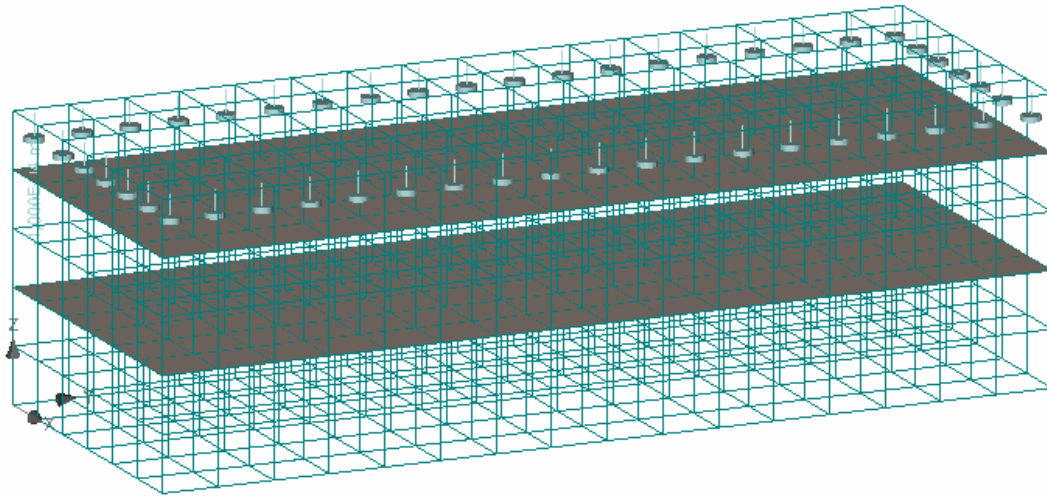


Figure 1-14: 3D model. Finite element mesh. Contact between steel plate and top concrete plate is rigid. Contact between two concrete plates is sliding interface. Vertical displacement is prescribed on the top surface of the steel plate in the loads case 1.

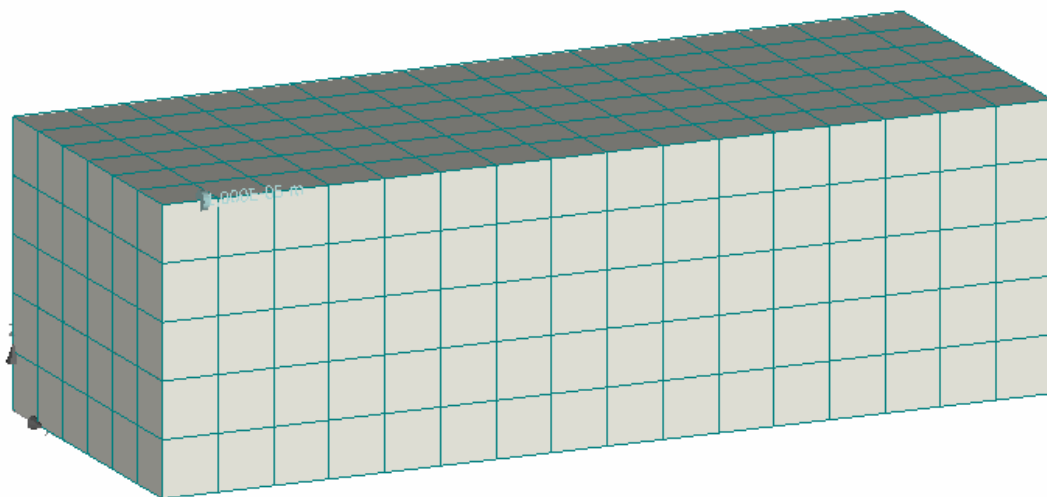


Figure 1-15: Mesh of the surface. Prescribed displacement in the top point of steel plate on the symmetry axes (represents midpoint of the whole specimen).

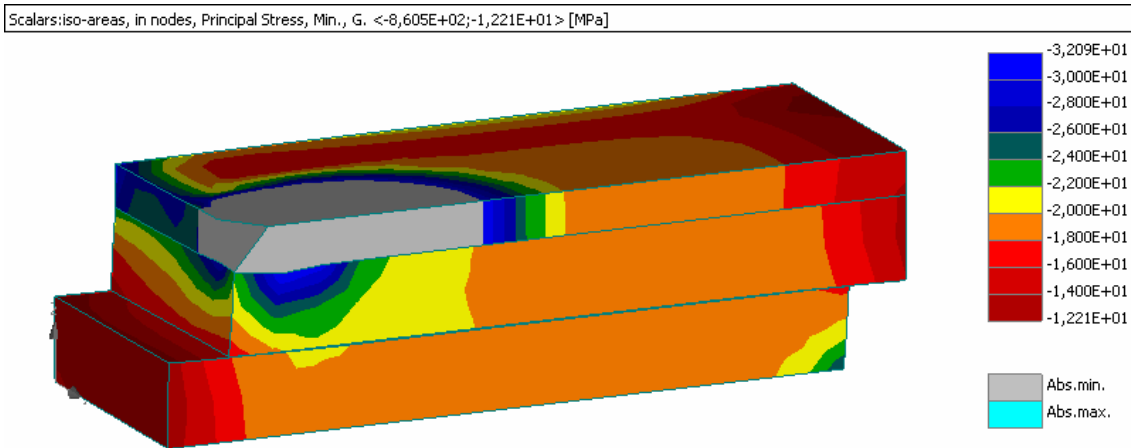


Figure 1-16: Deformed specimen. Shear displacement can be seen on the interface plane. Displacements magnified by factor 100. Principal compressive stress isoareas shown.

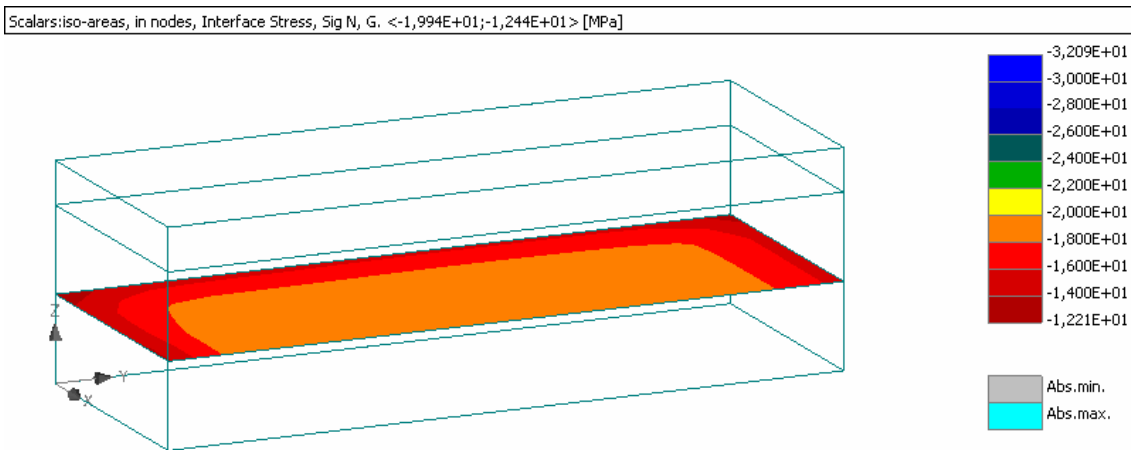


Figure 1-17: Normal contact stress in interface.

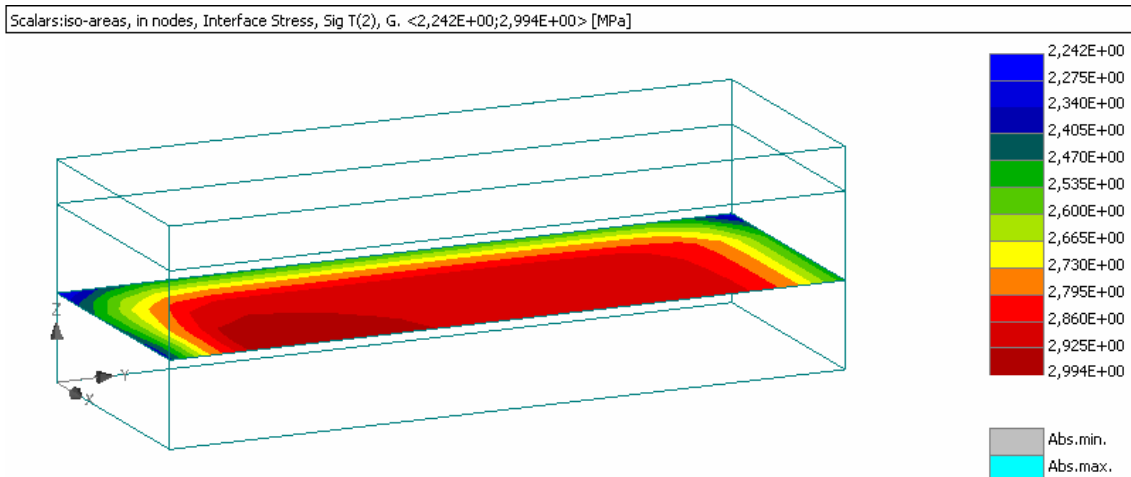


Figure 1-18: Shear contact stress in interface.

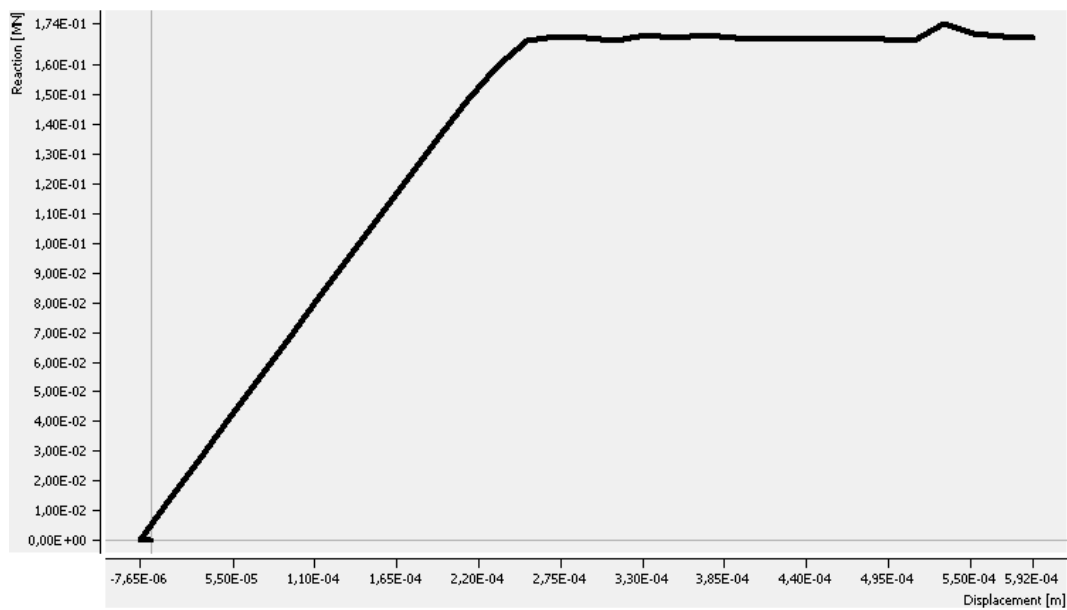


Figure 1-19: Load-displacement diagram.

A deformed shape of the specimen at and of test is shown in Figure 1-16. It clearly shows sliding of the interface. This is also indicated by horizontal shape of the load-displacement diagram in Figure 1-19. Maximum shear force to make interface sliding is about 0.17 MN (for symmetrical half of the specimen). The stress on the interface is not exactly uniform as can be seen from Figure 1-17 and Figure 1-18. The maximum normal stress is about -20 MPa (compression) and shear stress 3MPa. This agree with the material friction law of the interface

$$\tau_{\max} = c + \sigma_n \varphi = 1 + 0.1 \cdot 20 = 3 \quad (\text{MPa})$$

It can be observed, that for the prescribed vertical displacement $-0,07\text{mm}$ the normal contact stress -20Mpa is much higher comparing to 2D analysis (-15.3Mpa). This is due to 3D action, where lateral displacements are constrained by support conditions and top steel plate. This leads to high total maximal load which is $H=0.34$ MN in 3D, compared to 0.26 MN in 2D.

2 STRUCTURAL ELEMENTS ANALYSES

2.1 Beam on elastic foundation (SPRI)

Keywords: contact, nonlinear springs

Input files: SPRI\SPRI.cc2

2.1.1 Introduction

Two concrete beams are resting on a rigid foundation as shown in Figure 2-1. Each beam has a cross section of 300x200 mm. The top beam is supported by the bottom one. The bottom beam is supported on the bottom face by the rigid foundation. The top beam is loaded by a distributed force with a triangular distribution. The contact plane between the two beams is assumed to transmit only compression. In ATENA, the problem can be modeled in two ways.

The first way is to substitute the bottom beam by an elastic foundation. This model is used in this example. The behavior of the bottom beam is simplified since its plane stress continuum is substituted by the uniaxial springs of the Winkler foundation type. However, if the main concern of the analysis is the top beam, the simplification can be acceptable.

The second way, to model both beams as continuum and to define the contact plane as an interface, is not solved here.

2.1.2 Comments on FE model preparation

2.1.2.1 Materials

The material of the upper beam is represented using the SBETA concrete model with parameters listed in Table 2.1-1. In addition we have to define material properties of the springs representing the lower beam. To implement the assumption that the interface between the two beams may transfer only compression, we utilize the nonlinear spring material model. We define only the compressive branch of the spring stress-strain diagram by two points [-1 (-), -31720 (MPa)] and [0 (-), 0 (MPa)]. Outside the defined interval (i.e. in tension) the stress is considered to remain zero. Note, that the slope of the defined compressive branch corresponds to Young's modulus of concrete. This data is automatically converted by ATENA into spring constant (force vs. displacement relation) using the spring length and width provided through Springs option in Topology – Line definition window (see the next paragraph).

2.1.2.2 Topology

Springs representing the lower beam are defined through the Springs option for the bottom horizontal line. Here we input the direction, orientation (Global in negative Y), material and width and length of the springs.

2.1.2.3 Loads and supports and Run

The bottom side of the beam is supported by the springs. Hence no additional vertical supports are necessary. Symmetry of the problem is utilized, thus horizontal displacements are fixed along the vertical symmetry line. Loading on the top surface is applied as the Partial and quadrilateral type along the top line. The magnitude of the loading pattern is one tenth of the total load. Thus, load is applied in ten increments. The standard solution parameters are used.

2.1.3 Results

The maximum applied load does not cause any cracking or crushing of the concrete beam. However, as the load increases a portion of the beam is pressed down while another portion lifts up. Figure 2-2 shows the vertical displacements and the normal stress acting along the bottom line of the beam. The figure clearly indicates that the present model correctly represents the contact phenomena as no normal stresses are transferred where the interface opens up.

Table 2.1-1 Material properties of upper concrete beam

Material type		SBETA material	
Elastic modulus	E_c	31.72	GPa
Poisson's ratio	ν	0.2	-
Compressive strength	f_c	28.5	MPa
Tensile strength	f_t	1.6	MPa
Type of tension softening		Exponential	
Fracture energy	G_f	111.5	N/m
Crack model		Fixed	

Table 2.1-2 Solution parameters

Solution method	Newton-Raphson
Stiffness/update	Tangent/each iteration
Number of iterations	20
Error tolerance	0.010
Line search	on, with iterations

Table 2.1-3 Finite element mesh

Finite element type	Quadrilateral (CCIsoQuad)
Element shape smoothing	on
Optimization	Sloan

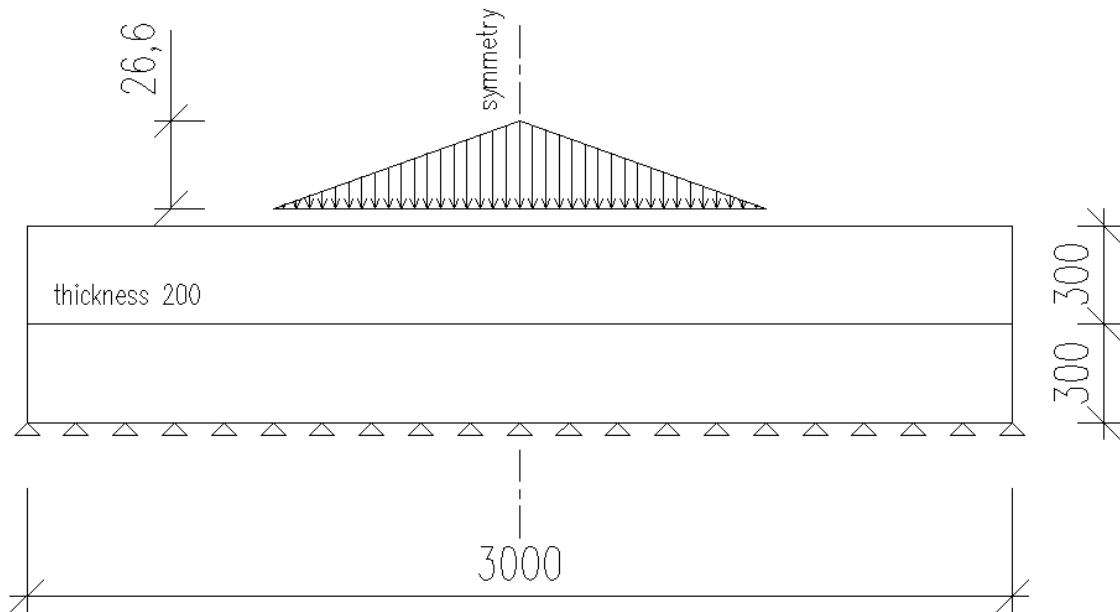


Figure 2-1: Geometry and boundary conditions of two-layer beam (dimensions in mm, loading in 10^{-2} MN/m)

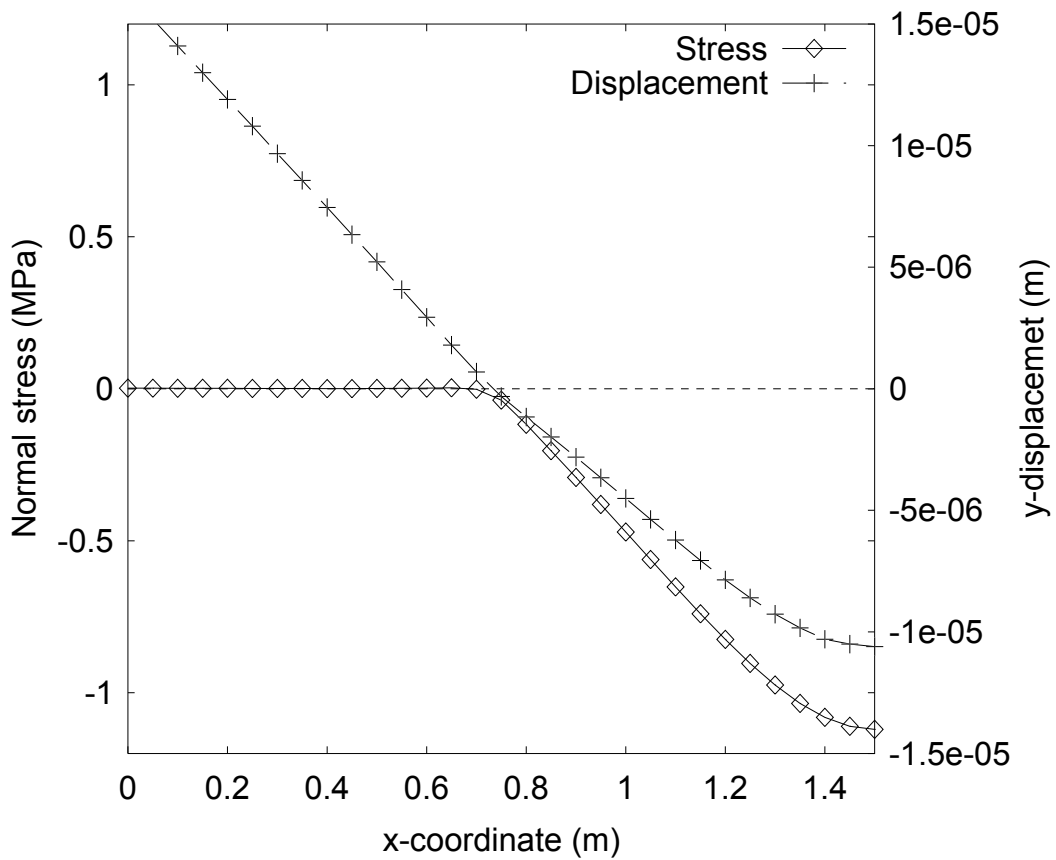


Figure 2-2: Vertical displacements and normal stress along the bottom of the beam

2.2 Simulation of tension stiffening experiment (TST)

Keywords: tension stiffening, concrete-reinforcement interaction, debonding, discrete reinforcement

Input files: TST\TSTF.cc2 (fixed crack model)
TST\TSTR.cc2 (rotated crack model)

2.2.1 Introduction

In this example we use ATENA to reproduce the tension stiffening effect of reinforced concrete elements. This effect, which is a demonstration of post-cracking interaction of concrete and reinforcement, may be observed well when tension is applied to a single reinforcement bar embedded in a concrete prism (Figure 2-3). Prior to concrete cracking, both concrete and reinforcement bar fully contribute to the stiffness of the specimen (Figure 2-5, Figure 2-6). Once concrete starts to crack, its contribution decreases but the specimen stiffness is still higher than that of a bare reinforcement bar. This is due to concrete pieces between cracks constraining the bar elongation. In some programs for FE analysis of reinforced concrete, this phenomenon is included by introducing a separate material property. In ATENA, though, this is not necessary and the tension stiffening effect is reproduced by properly modeling discrete reinforcement and cracking in the surrounding concrete. To demonstrate the way ATENA treats tension stiffening, we reproduce an experiment by Hartl [1].

2.2.2 Comments on FE model preparation

The experimental setup is shown in Figure 2-3. For the analysis, we adopt a two-dimensional plane stress idealization of the problem. We utilize symmetry, which allows us to model only one fourth of the specimen, while appropriately introducing displacement boundary conditions (Figure 2-4).

2.2.2.1 Materials

The SBETA material model is employed for concrete. Material parameters are listed in Table 2.2-1. Analyses are carried out with both fixed and rotated crack models to compare performance of the two approaches. Reinforcement is modeled as elastic perfectly-plastic material (Table 2.2-2).

2.2.2.2 Topology

In order to adequately capture concrete cracking, we use a relatively fine mesh with the element size of 5mm. The discrete reinforcement is modeled by a single segment line placed along x-axis. The bar cross-sectional area is set to one half of the real one to account for symmetry. The FE model is shown in Figure 2-4.

2.2.2.3 Loads and supports and Run

The load case LC1 contains the fixed-displacement boundary conditions along

symmetry lines. Loading (LC2) is applied by prescribing horizontal force increments of 2 or 4 kN in the joint placed on the right end of the rebar. Since we want to trace the load-displacement curve of the specimen even beyond the limit when it becomes perfectly plastic (i.e., applied force may no longer increase), we employ the arc length control method, with parameters listed in Table 2.2-3.

2.2.3 Results

The computed load-displacement curves are shown in Figure 2-5 and Figure 2-6. It is seen that the analytical results obtained with both fixed and rotated crack models closely match the range of experimental results. The solution with the fixed crack model is closer to the upper bound of experimental data and the one with the rotated crack model is closer to the lower bound.

Figure 2-7 and Figure 2-8 show the computed crack patterns and the deformed specimen shapes. In both figures we can see formation of several large cracks, perpendicular to the tension direction. The main difference between results with the fixed and rotated crack models is in the number of these cracks (4 vs. 2). Also, the rotated crack model produced localized cracks in the concrete adjacent to the reinforcing bar. This can be interpreted as the separation of concrete and reinforcement or the bond failure. Quantitative results are compared in the following table:

	Number of cracks per half length	Average crack width (mm)
Analysis – fixed crack	4	0.10
Analysis – rotated crack	2	0.20
Experiment	2	0.16

2.2.4 References

[1] Hartl, G., Die Arbeitslinie Eingebetteter Stähle bei Erst- und Kurzzeitbelastung, Dissertation, University of Innsbruck, 1977

Table 2.2-1 Material properties of concrete

Material type		SBETA material	
Elastic modulus	E_c	29	GPa
Poisson's ratio	ν	0.2	-
Compressive strength	f_c	22.95	MPa
Tensile strength	f_t	3.1	MPa
Type of tension softening		Exponential	
Fracture energy	G_f	58	N/m
Crack model		Fixed/rotated	

Table 2.2-2 Material properties of reinforcement rod $\varnothing 12$

Material type		Reinforcement	
		bilinear	
Elastic modulus	E	210	GPa
Yield strength	σ_y	460	MPa
Hardening		perfectly plastic	

Table 2.2-3 Solution parameters

Solution method		Arc length	
Stiffness/update		Tangent/each iteration	
Number of iterations		50	
Error tolerance		0.001	
Arc length	Method	Crisfield	
	Adjustment method	Variable conservative 1/4	
	Load/disp. ratio	0.2 (constant)	
Line search		on, with iterations	

Table 2.2-4 Finite element mesh

Finite element type	Quadrilateral (CCQ10SBeta)	
Element shape smoothing	on	
Geometrical nonlinearity	on	
Optimization	Sloan	

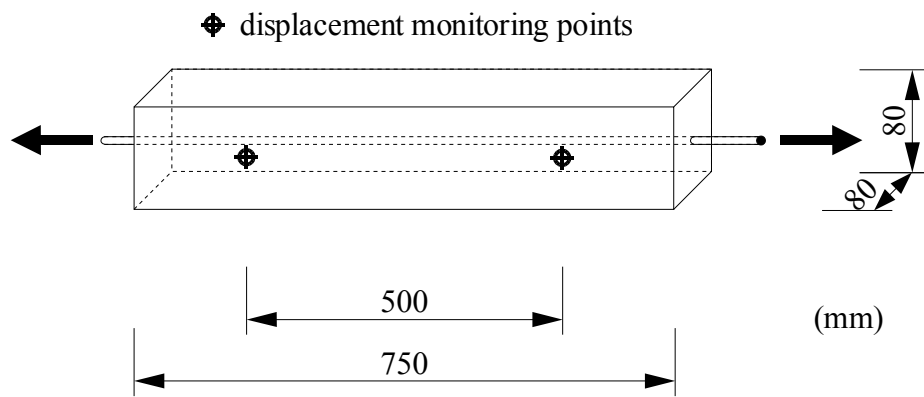


Figure 2-3: Arrangement of tension-stiffening experiment [1]

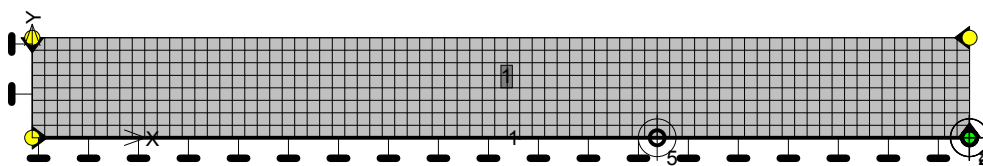


Figure 2-4: Finite element model

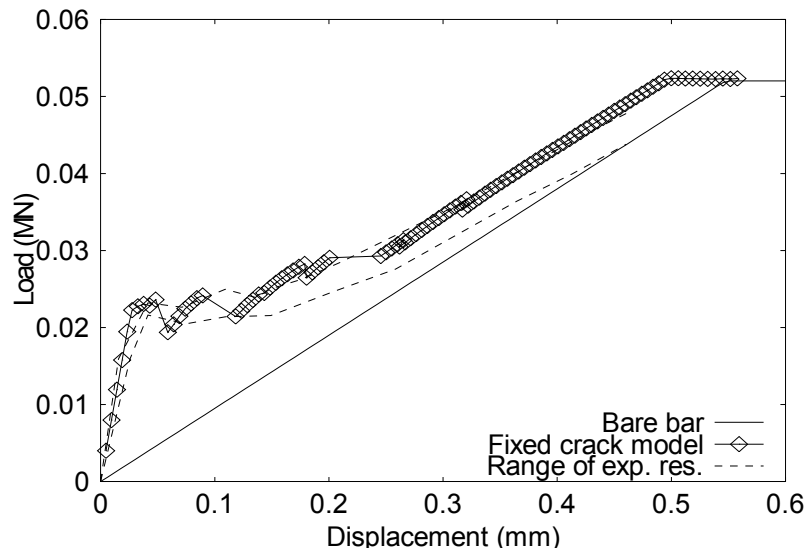


Figure 2-5: Load-displacement curves of tension-stiffening specimen (fixed crack model)

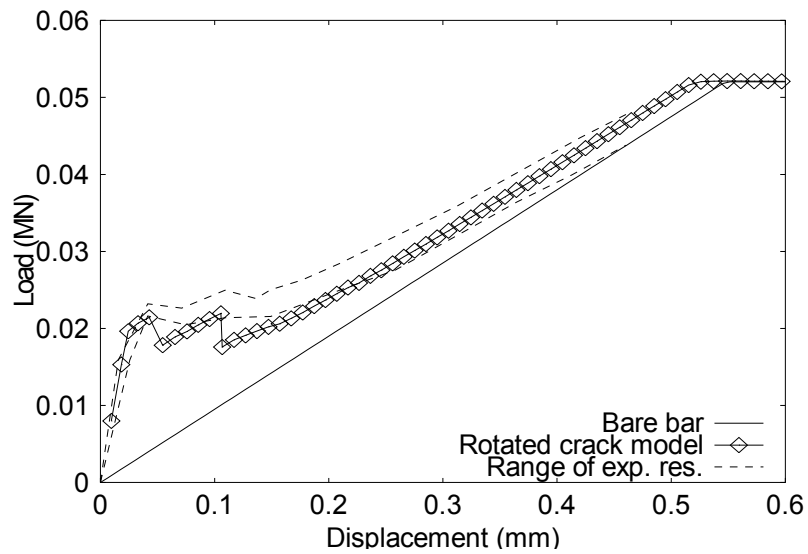


Figure 2-6: Load-displacement curves of tension-stiffening specimen (rotated crack model)

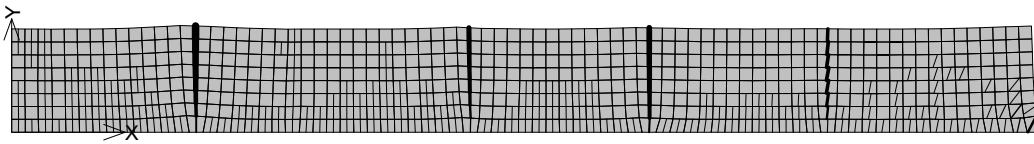


Figure 2-7: Computed crack pattern and deformed shape at displacement of 0.47 mm (fixed crack model). Only cracks wider than $1\ \mu\text{m}$ are plotted.

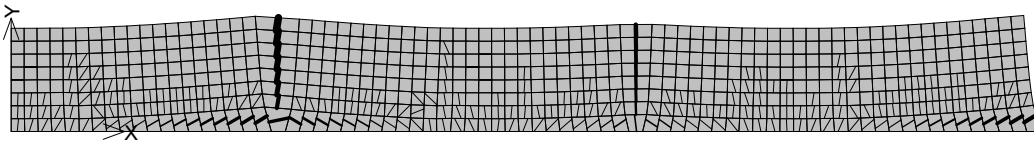


Figure 2-8: Computed crack pattern and deformed shape at displacement of 0.47 mm (rotated crack model). Only cracks wider than $1\ \mu\text{m}$ are plotted.

2.3 Simulation of tension stiffening experiment (TST) 3D

Input files: TST\TSTF.cc3 (fixed crack model in 3D)

2.3.1 Introduction

In this example we use ATENA 3D environment to reproduce the tension stiffening effect of reinforced concrete elements. The geometry and material properties are the same as in 2D example.

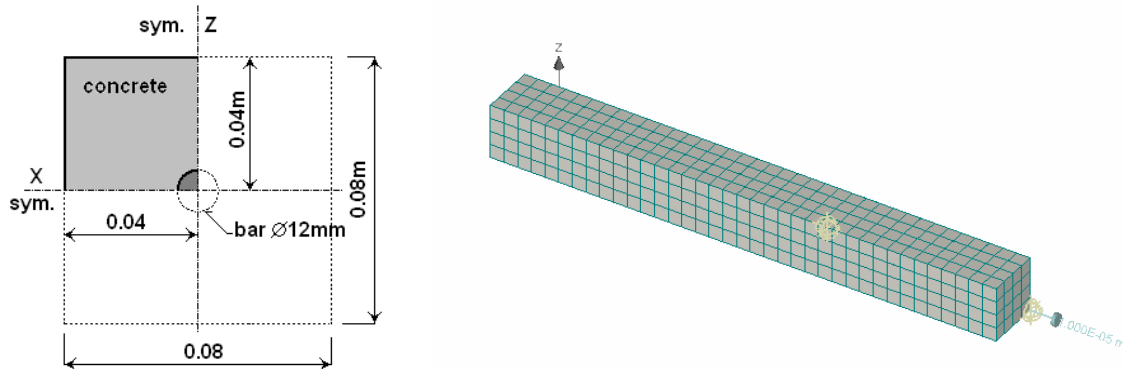


Figure 2-9: 3D model. Symmetrical section, finite element mesh.

2.3.2 Comments on FE model preparation

The experimental setup is shown in Figure 2-3. For the analysis, we use three-dimensional stress analysis. We utilize symmetry, which allows us to model only 1/8 of the specimen, while appropriately introducing displacement boundary conditions on symmetry axes.

2.3.2.1 Materials

The ATENA material model 3D Nonlinear Cementitious 2 is employed for concrete. Material parameters are listed in Table 2.2-1. Analysis is carried out with fixed crack model. Reinforcement is modeled as elastic perfectly-plastic material (Table 2.2-2).

2.3.2.2 Topology and mesh

Prismatic geometry represents one quarter of the test specimen. The discrete reinforcement is modeled by a single segment line placed in the cross section corner (which is the center of full cross section). Bar direction is parallel with Y-axis. The bar cross-sectional area is set to 1/4 of the real one to account for symmetry. The element size is 10mm, which is twice the element size in 2D. Isoparametric brick elements with 8 nodes, 3 DOFs in node, and 8 integration points are used. The FE model is shown in Figure 2-9.

2.3.2.3 Loads, supports and solution parameters

Two load cases are defined. The load case no.1 “Supports” contains displacement boundary conditions along symmetry planes. The loading is imposed as prescribed displacement at the bar end in the load case no.2 “Prescribed displacement”. The value

of displacement in the load case 1 is 0.00001 in Y direction.

Load history consists of 51 load steps (analysis steps) each with load cases 1 and 2. Note that load steps in ATENA are incremental, which means that the load intensity in a current load step is added to the previously applied loads. Standard Newton-Raphson method is user. Equation solver is standard (direct elimination).

Monitoring points are defined in order to simulate structural response:

Monitor 1 – “Disp 1” is displacement Y at the specimen end on bar location.

Monitor 2 – “Disp 2” is displacement Y located on concrete surface at distance 250 mm from the specimen center. It corresponds to the gauge location in experiment. However, displacement over only half of the length is measured in analysis due to symmetry. Therefore, experimental displacements must be reduced by factor 0.5 for comparison.

Monitor 3 – “Reaction” is the reaction force at the point of prescribed displacement. Note, that due to symmetry reduction of specimen size the reaction represents $\frac{1}{4}$ of the force measured in actual test.

2.3.2.4 Results

The resulting load-displacement curve is shown in Figure 2-10. This curve was plotted in Excel using data from ATENA. The displacement is measured in monitor 2 and monitored force is multiplied by factor 4 in order to represent the total force.

Resulting damage state is evaluated in the load step 51, which is near yielding point of steel bar and after completing the crack development. The stress and crack state at the load step is shown in Figure 2-11. For the crack picture we used the crack width filter with limit width 0.00001m. This means that fine cracks below given limit are not displayed. Two major open cracks can be observed. They pass throughout the entire cross section and are almost stress free. The crack width on the surface is displayed on a separate graphics in Figure 2-12, from which we can read the crack widths values 0,17 and 0,09 mm for the 1st and 2nd cracks, respectively.

Deformed mesh shows opening of cracks in Figure 2-11. Magnifying factor 100 is used to make the deformed form visible. This figure also shows iso-areas of tensile principal stress in concrete, which indicates how the tension stiffening effect works. The concrete between cracks is subjected to the tensile stress, which generates tension stiffening. This is also indicated by distribution of stress in bar, Figure 2-14, where the highest stress in crack is 412 MPa and between cracks it reduces to 296 MPa.

Display of cracks inside the concrete, Figure 2-13, shows that major cracks are almost planar. Additional cracks appear near the end, where the load is applied and along the bar near the end. The later indicate a bond deterioration of concrete and proves, that some bond behavior is presented by concrete damage providing that sufficiently small elements are used.

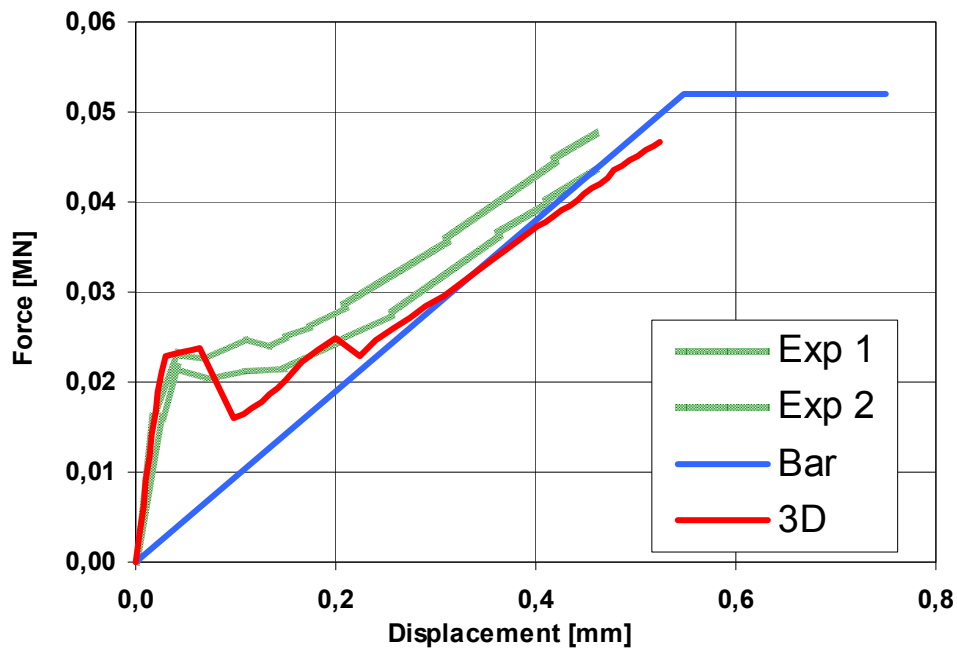


Figure 2-10: Load-displacement diagram.

In high load range the 3D analysis shows weaker response than bar itself. This can be explained by bond failure modeled by splitting cracks mentioned above. The bond slip of bar is also visible from a mesh distortion near the bar in Figure 2-11.

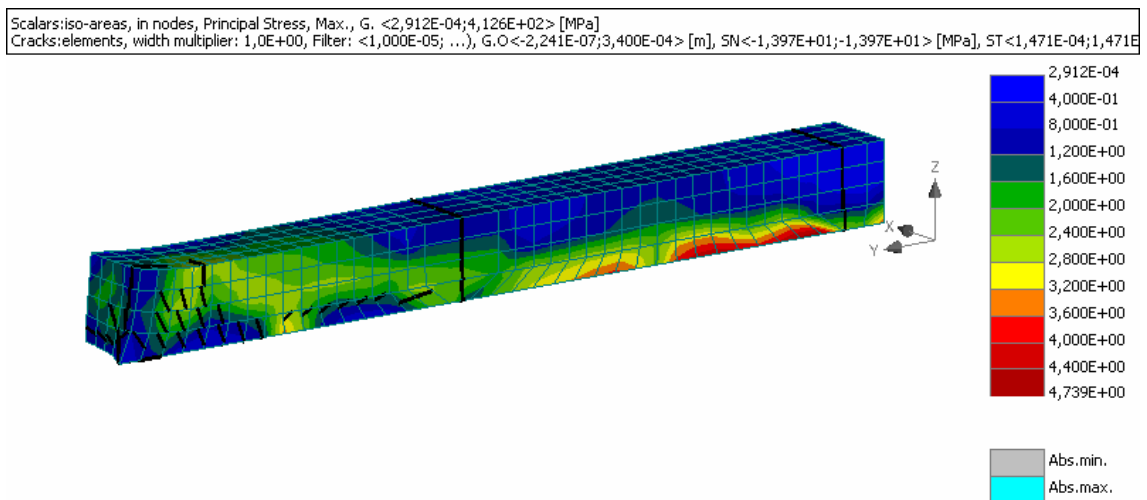


Figure 2-11: Damage state. Deformed mesh, crack pattern, tensile stress iso-areas.
Load step 51, displacement (at Monitor2) 0,00054m, force (1/4) 0.0117 MN.

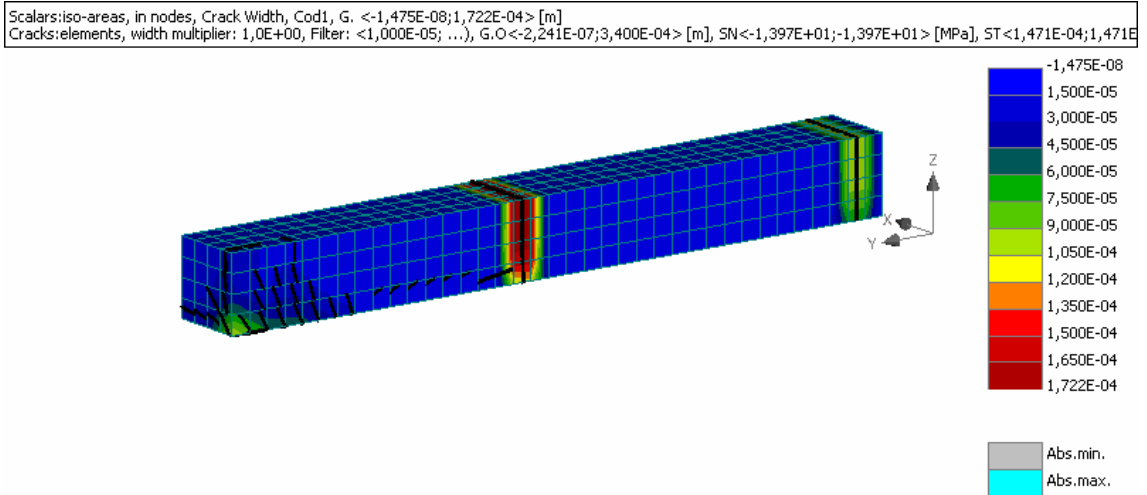


Figure 2-12: Crack width iso-areas at load step 51. Undeformed mesh.

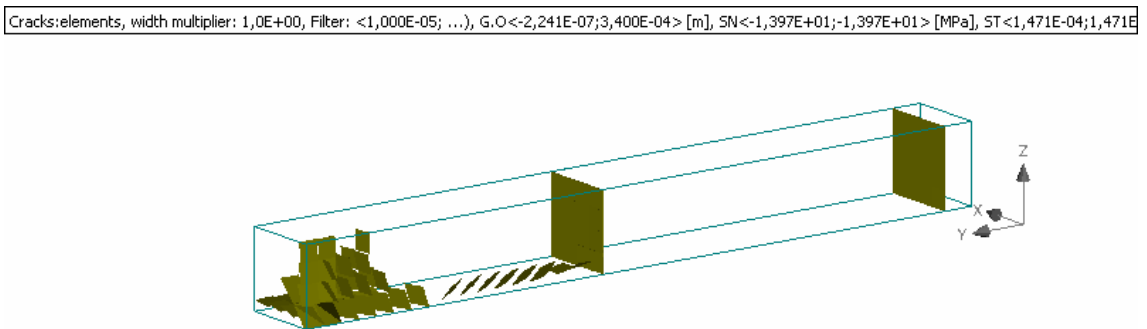


Figure 2-13: Cracks inside of concrete at load step 51.

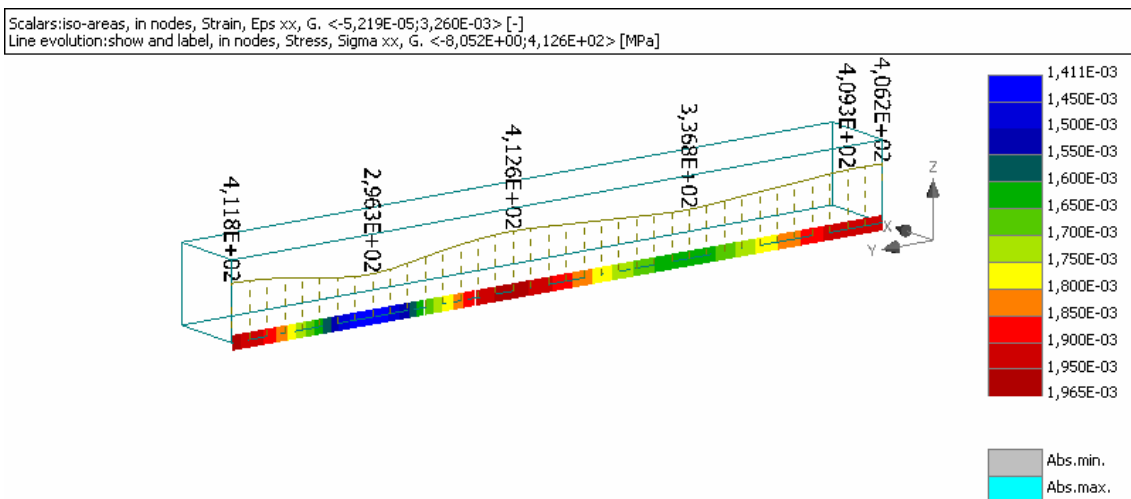


Figure 2-14: Stress (labeled distribution) and strains (isoareas) in bar at load step 51.

2.4 Leonhardt's shear beam (LSB)

Keywords: reinforced concrete, shear failure, discrete reinforcement, quadrilateral/triangular elements

Input files: LSB\LSBI.cc2 (CCIsoQuad)
 LSB\LSBQS.cc2 (CCQ10Sbeta)
 LSB\LSBT.cc2 (Triangular)

2.4.1 Introduction

This example shows a simply supported reinforced concrete beam, which fails in shear. The beam had been earlier experimentally tested by Leonhardt and Walther [1]. The effect of the finite element type on the reproduction of the beam response is also investigated.

The geometry, reinforcement, and configuration of the tested beam are shown in Figure 2-15. Its dimensions are 2550×320×190 mm. There are two longitudinal reinforcement bars $\varnothing 26$, with total cross-sectional area 1060 mm² and cover 37 mm. The beam lacks any vertical reinforcement (hoops and ties). Loading is by two forces, symmetrically located. The loading forces and supports are applied through steel plates to avoid local crushing.

2.4.2 Comments on FE model preparation

2.4.2.1 Materials

Concrete is represented by the SBETA material model. Relevant material properties are listed in Table 2.4-1. Reinforcement is modeled as elastic perfectly-plastic material (Table 2.4-2). The loading and support steel plates are assumed to remain elastic, with Young's modulus 200 GPa and Poisson's ratio 0.3.

2.4.2.2 Topology

The model for computer analysis is taking advantage of symmetry. Only half of the beam is considered and the symmetry axis is simulated by boundary conditions with constrained horizontal displacements. As in the physical experiments, loads and vertical support constraints are applied through steel plates to avoid local concrete crushing. The plates are assumed perfectly bonded to concrete.

As we intend to compare results obtained with different element types, meshing is performed using either quadrilateral "CCIsoQuad", "CCQ10Sbeta" or triangular "Triangle" element types. It is recommended to use a fine uniform mesh (element size 0.025 m for quadrilaterals and 0.03 m for triangles is prescribed throughout the beam) in order to minimize the effect of FE discretization on formation and propagation of cracks, namely the inclined shear ones.

Reinforcement is modeled by a single straight line in a discrete way ("bar reinforcement").

2.4.2.3 Loads and supports and Run

Loading is applied by prescribing vertical displacement at the middle point on top of the loading plate in constant increments of 0.1 mm. The Newton-Raphson solution method with parameters listed in Table 2.4-3 is employed.

The overall response is recorded at two monitoring points – loading as the reaction at the top loading point and deflection at the bottom of the beam on the symmetry plane.

2.4.3 Results

Global response of the beam under given two-point loading can be observed from the load-displacement diagram in Figure 2-16. This figure compares the analytical diagrams and the experimental one. The experimental curve represents the average of two tests. It follows from the comparison of responses that all the analyzed meshes give consistent results in deflections as well as in maximum loads. They also compare well with the experiments, although the analytically reproduced peak loads are somewhat higher. It should be noted, though, that the experimental results also show a big scatter, as it is evident in the following table.

	Peak load (kN)	Peak deflection (mm)
Analysis, CCIsoQuad elem.	84.34	3.644
Analysis, CCQ10Sbeta elem.	85.83	3.651
Analysis , Triangular elem.	84.49	3.341
Experiment 1	60	2.57
Experiment 2	76.5	3.6*)

*) extrapolated value

The computed and experimentally observed crack patterns are shown in Figure 2-18, Figure 2-19, Figure 2-20, and Figure 2-17. All analytical crack patterns show a similar diagonal crack path, which compares well with the experimental one. The analytical failure mode was due to formation of a diagonal crack, which caused kinematic collapse of the beam. The reinforcement was not yielding and compressive strength of concrete was reached only in small areas near the loading plate.

The study illustrates the objectivity of the brittle mode of failure. The crack band method used in the program for crack modeling, which is based on fracture energy, gives results, which are not very sensitive to the finite element mesh. This conclusion is valid for deflections (stiffness of the structure), peak loads, as well for crack patterns.

2.4.4 References

[1] “Schubversuche an einfeldrigen Stahlbetonbalken mit und ohne Schubbewehrung, Deutscher Ausschuss für Stahlbeton, Heft 151, Berlin 1962, Ernst&Sohn”

Table 2.4-1 Material properties of concrete

Material type		SBETA material	
Elastic modulus	E_c	31.72	GPa
Poisson's ratio	ν	0.2	-
Compressive strength	f_c	28.48	MPa
Tensile strength	f_t	1.64	MPa
Type of tension softening		Exponential	
Fracture energy	G_f	100.0	N/m
Crack model		Fixed	

Table 2.4-2 Material properties of reinforcement

Material type		Reinforcement bilinear	
Elastic modulus	E	208	GPa
Yield strength	σ_y	560	MPa
Hardening		perfectly plastic	

Table 2.4-3 Solution parameters

Solution method	Newton-Raphson	
Stiffness/update	Tangent/each iteration	
Number of iterations	40	
Error tolerance	0.010	
Line search	on, with iterations	

Table 2.4-4 Finite element mesh

Finite element type	Quadrilateral (CCIsoQuad or CCQ10Sbeta) or Triangular	
Element shape smoothing	on	
Optimization	Sloan	

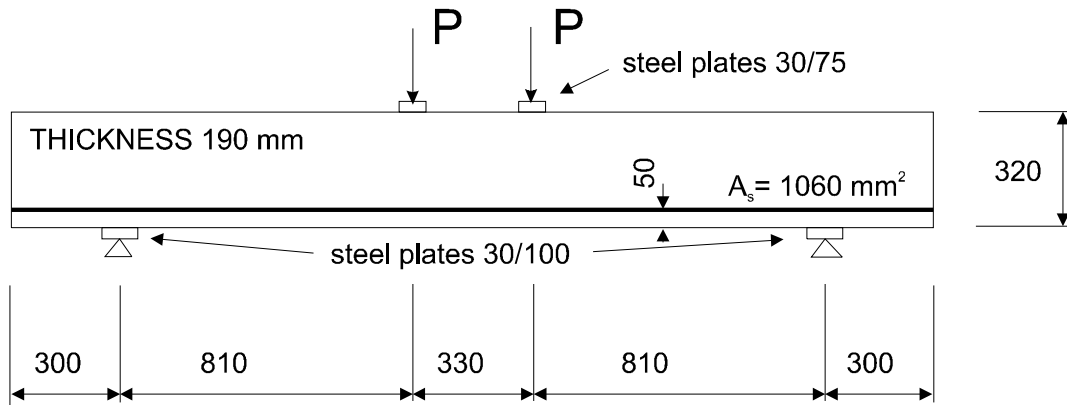


Figure 2-15: Geometry of the Leonhardt's beam no.5.

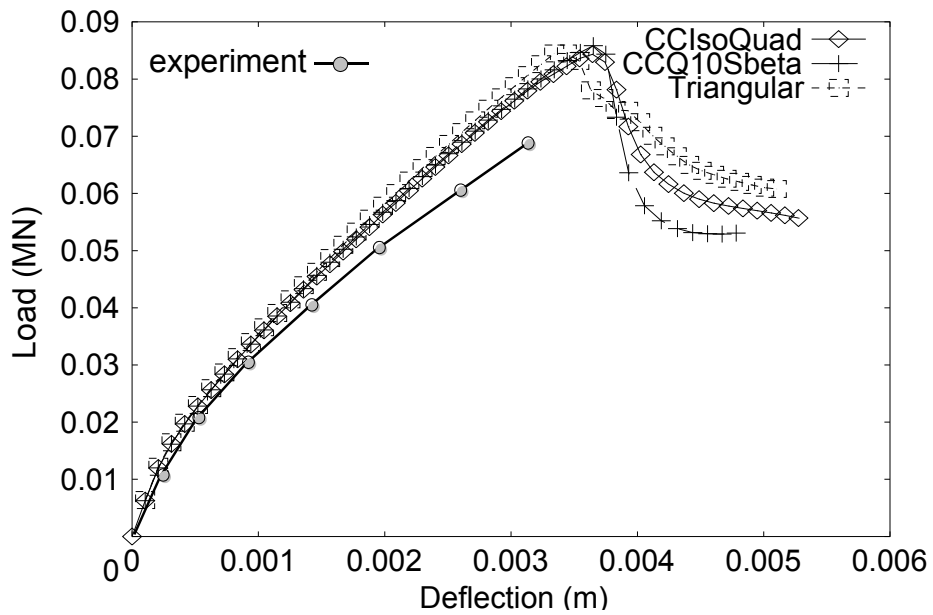


Figure 2-16: Load-displacement curves of shear beam

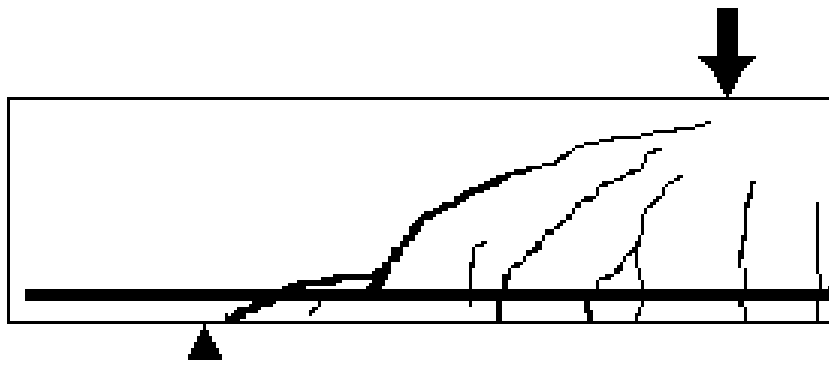


Figure 2-17: Crack pattern as observed in the experiment

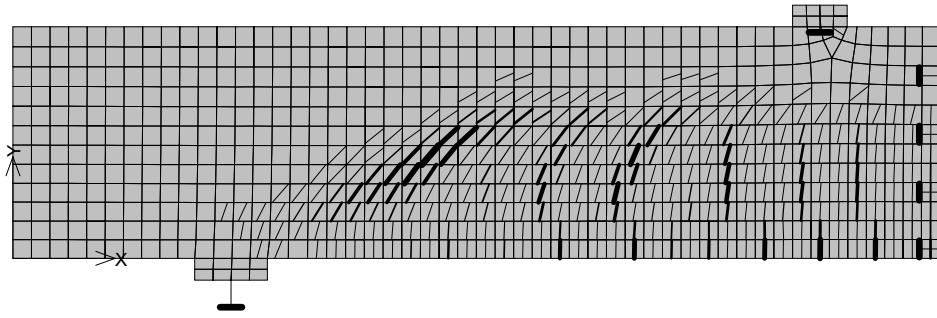


Figure 2-18: Crack pattern around peak load obtained with quadrilateral mesh – CCIsoQuad (Step 34)

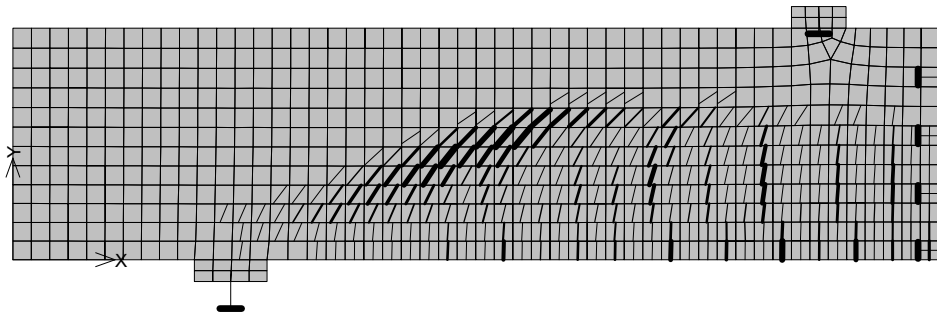


Figure 2-19: Crack pattern around peak load obtained with quadrilateral mesh – CCQ10Sbeta (Step 35)

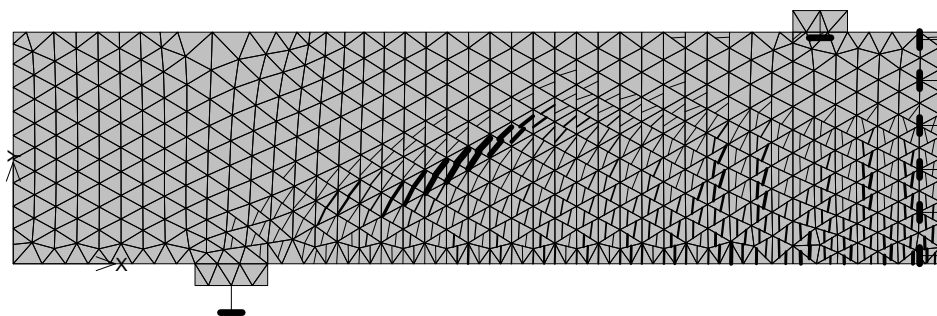


Figure 2-20: Crack pattern around peak load obtained with triangular mesh (Step 33)

2.5 Leonhardt's shear beam (LSB) 3D

Geometry and reinforcement is taken from experiment described in 2D example above. Material parameters are the same. For concrete material CC3DNonLinCementitious2 is used. Finite element model is shown in Figure 2-21. Two cases are analyzed one with perfect bond other with CEB bond model.

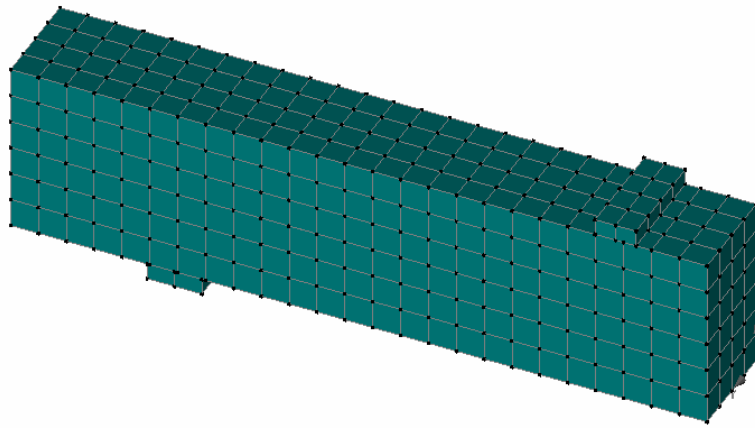


Figure 2-21: Finite element model.

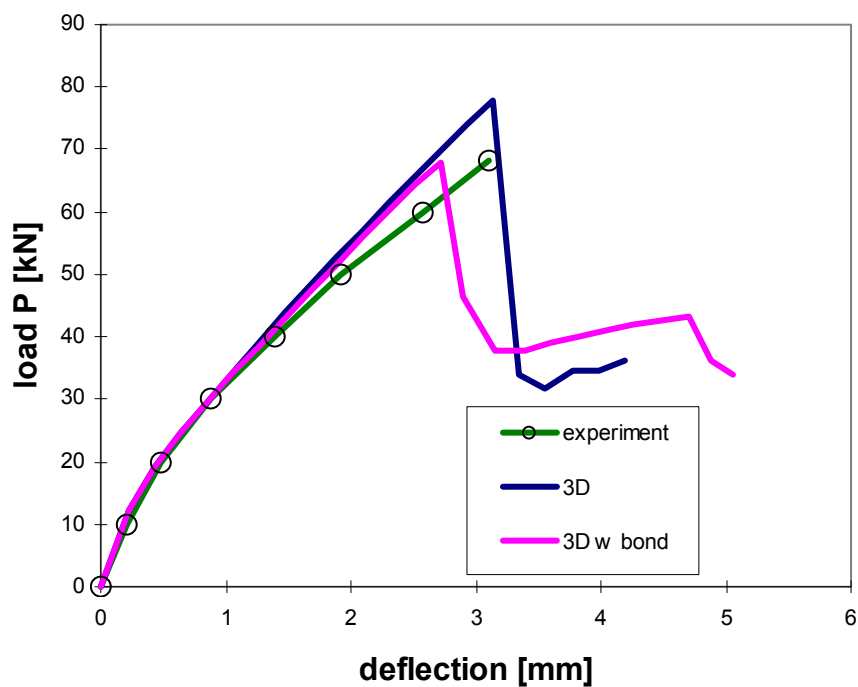


Figure 2-22: Load-displacement diagram.

The comparison of load-displacement diagrams for two 3D models (with and without

bond slip) and experiment by Kupfer (see reference in 2D example) is shown in Figure 2-22.

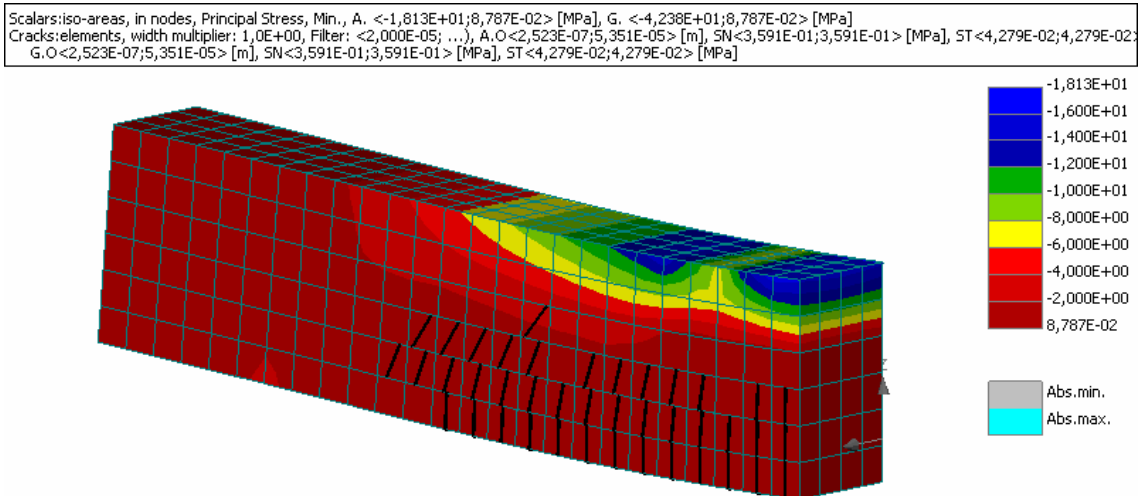


Figure 2-23: Stress and crack state at LS 11.

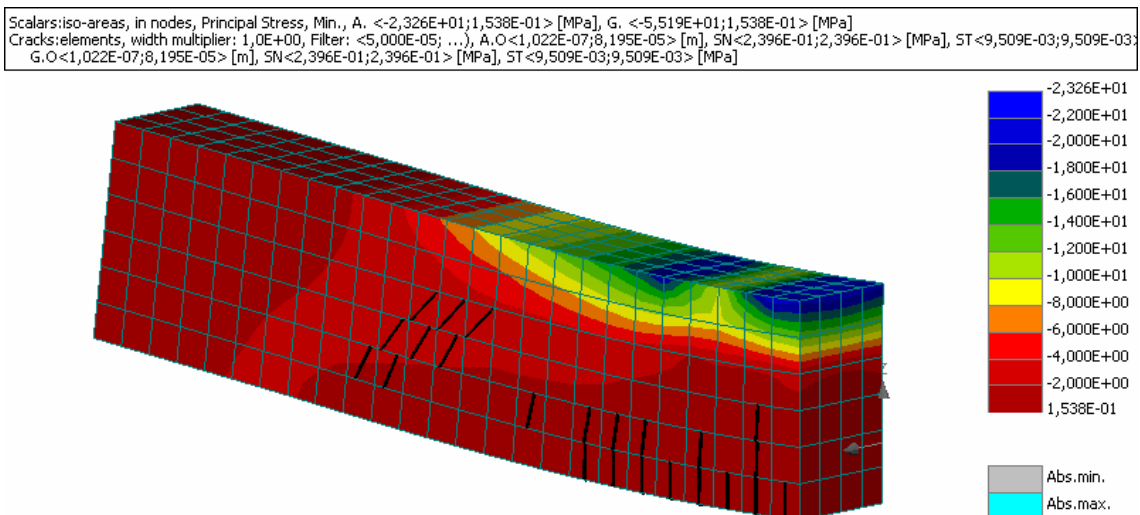


Figure 2-24: Stress and crack state at LS 15, before peak load.

Pictures of stress and cracks are showing only concrete. This is made with the use of “activity” in which only concrete macroelement is selected. In this way the stress range is not distorted by high stresses in loading plates.

The picture show states under ... before failure (load step 15) and after failure (load step 17). Cracks are subjected to filter

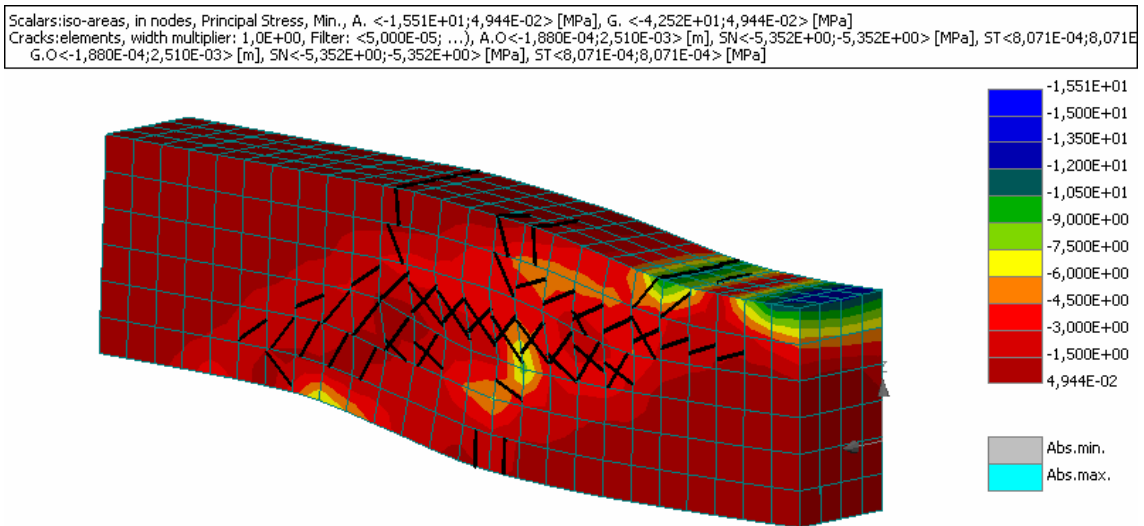


Figure 2-25: Stress and crack state at LS 17, after failure.

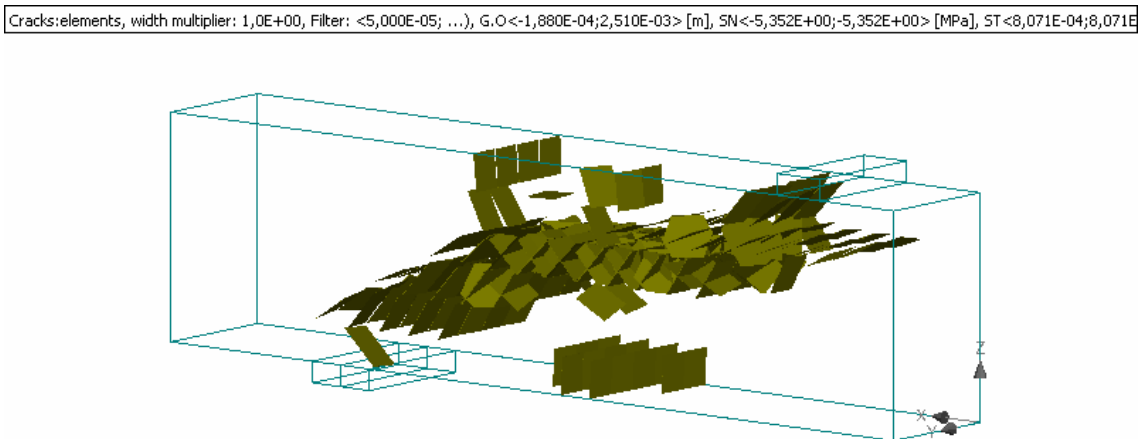


Figure 2-26: Failure cracks inside at LS 17.

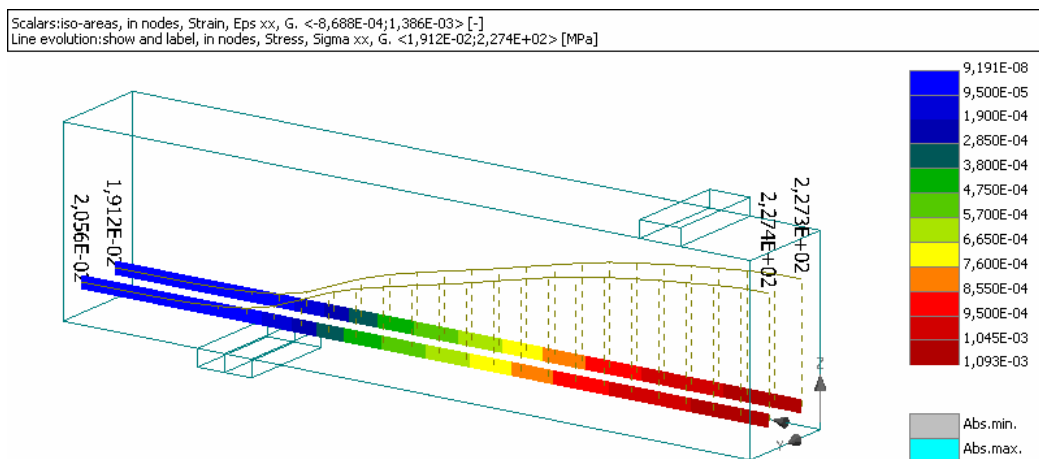


Figure 2-27: Stress (distribution) and strain (iso-areas) in reinforcement prior failure.

2.6 Prestressed concrete beam (INTB)

Keywords: reinforced concrete, discrete reinforcement, prestressing by internal cables, section plots

Input files: INTB\INTB.cc2

2.6.1 Introduction

This example shows a concrete beam with T-shaped cross section, prestressed by internal cables. Prestressing by the pre-tensioning method is applied in an unloaded stage, then cables are fully bonded and loading is applied. Therefore, under loading the deformation of the cables is fully compatible with that of concrete.

The geometry of the beam is shown in

Figure 2-28. The cross section of the beam is shown on the right side of the figure. The loading points and support rollers are equipped with steel plates to avoid stress concentration and local failures.

A beam with the same geometry, but external cables, shall be solved in the next example.

2.6.2 Comments on FE model preparation

2.6.2.1 Materials

Concrete is represented by the SBETA material model with material parameters listed in Table 2.6-1. Reinforcement is modeled as elastic perfectly-plastic material (Table 2.6-2). The loading and support steel plates are perfectly bonded to concrete and are assumed to remain elastic, with Young's modulus 210 GPa and Poisson's ratio 0.3.

2.6.2.2 Topology

The beam consists of several macroelements in order to allow prescribing different thickness of the beam wall and rim. Reinforcement is modeled as discrete one by three straight lines touching one another at their end-points.

2.6.2.3 Loads and supports and Run

Bottom supports are prescribed as the load case LC1 in all steps of the analysis. The first loading step corresponds to prestressing. In this step, total prestressing force of 0.2205 MN (corresponding to prestress of 450 MPa) is applied to all three reinforcement lines (LC3). Consequently, vertical loading is applied by prescribing vertical displacement at the upper loading plates in constant increments of 0.5 mm. The Newton-Raphson solution method with parameters listed in Table 2.6-3 is employed.

The overall response is recorded at two monitoring points – loading (as the reaction) at the right loading point and deflection at the same location. To facilitate plotting of internal forces, cross-sectional stress and strain distributions, and stress and strain distribution along the beam bottom edge, appropriate moment lines and cuts are specified.

2.6.3 Results

The computed load-displacement curve is shown in Figure 2-29. Deformed shapes and crack patterns at loading steps 12 (during hardening) and 100 (post-peak) are provided in Figure 2-30 and Figure 2-31, resp. In addition, Figure 2-32 shows distribution of xx -component of strain along predefined cut-lines at load step 100.

Table 2.6-1 Material properties of concrete

Material type		SBETA material	
Elastic modulus	E_c	33	GPa
Poisson's ratio	ν	0.2	-
Compressive strength	f_c	53.8	MPa
Tensile strength	f_t	3.392	MPa
Type of tension softening		Exponential	
Fracture energy	G_f	183.3	N/m
Crack model		Fixed	

Table 2.6-2 Material properties of prestressing cable

Material type		Reinforcement	
		bilinear	
Elastic modulus	E	200	GPa
Yield strength	σ_y	1600	MPa
Hardening		perfectly plastic	
Total cross-sectional area		$4.9 \cdot 10^{-4}$	m^2

Table 2.6-3 Solution parameters

Solution method	Newton-Raphson	
Stiffness/update	Elastic/each step	
Number of iterations	30	
Error tolerance	0.010	
Line search	on, with iterations	

Table 2.6-4 Finite element mesh

Finite element type	Quadrilateral (CCQ10Sbeta)	
Element shape smoothing	on	
Optimization	Sloan	

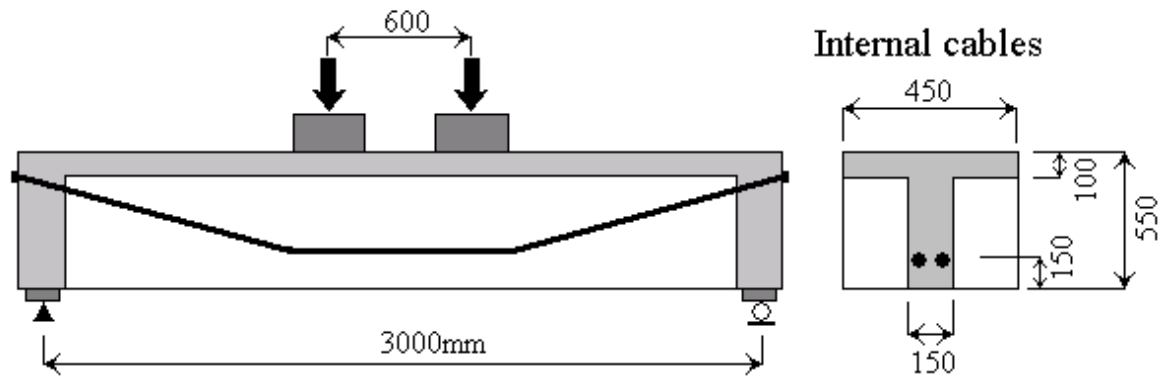


Figure 2-28 Beam prestressed by internal cables

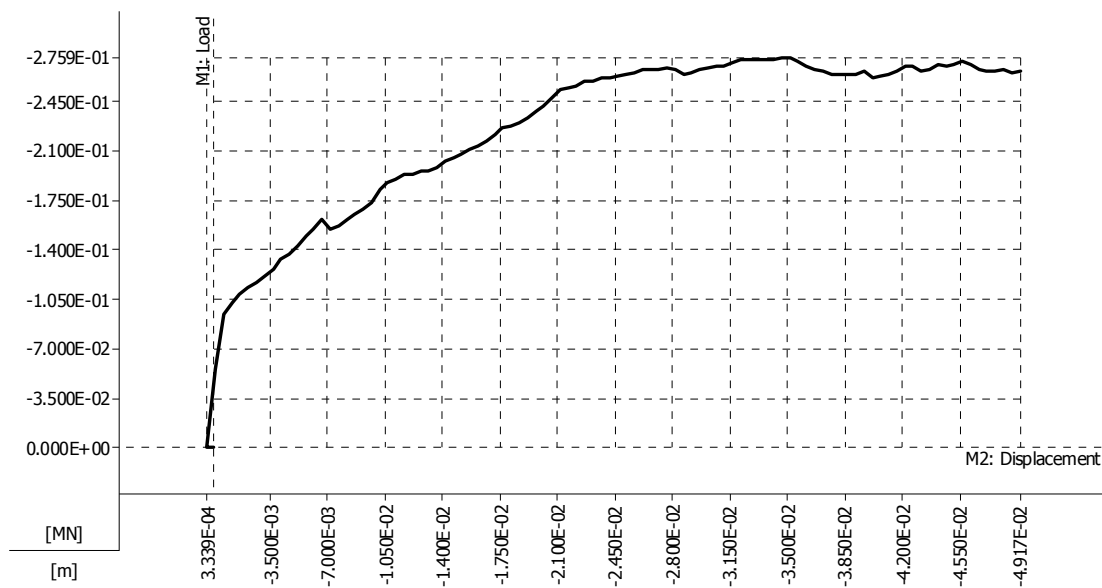


Figure 2-29 Computed load-displacement curve of beam with internal cables

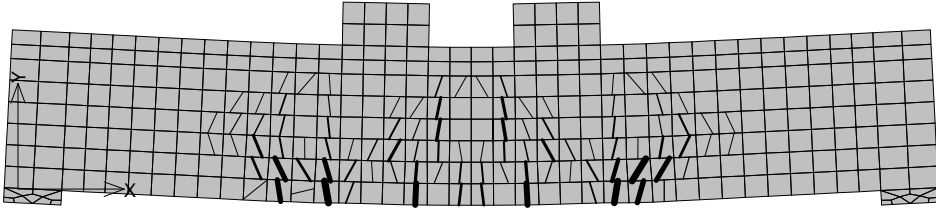


Figure 2-30 Computed crack pattern at load step 12

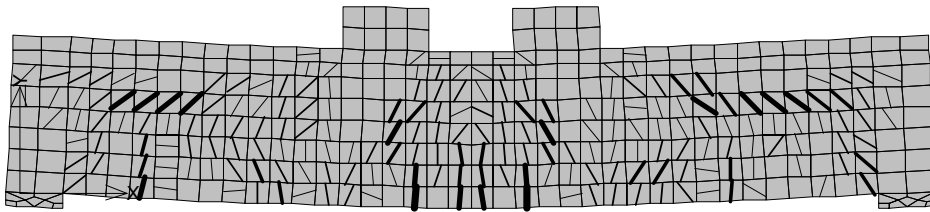


Figure 2-31 Computed crack pattern at load step 100

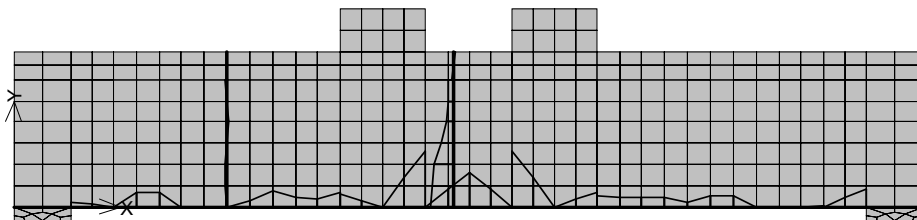


Figure 2-32 Distribution of engineering strain (xx -component) along predefined cut lines at load step 100

2.7 Prestressed concrete beam (INTB) 3D

Input file: INTB.cc3

The same beam as considered in the previous case of 2D analysis is subjected to 3D analysis. Its model is shown in Figure 2-33.

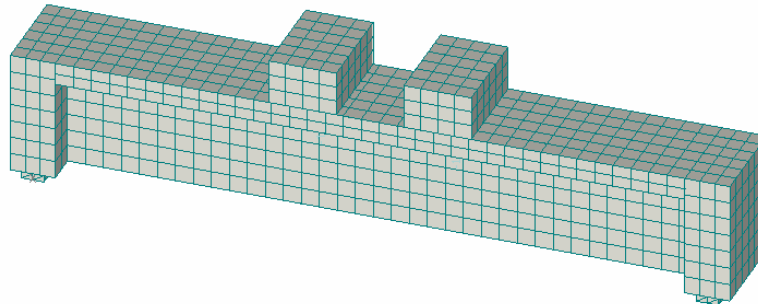


Figure 2-33 Finite element model.

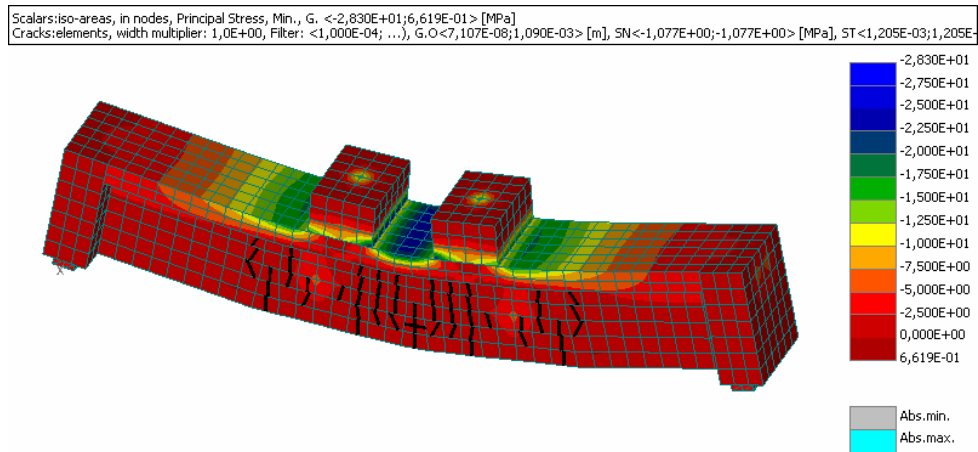


Figure 2-34 Stress and crack state.

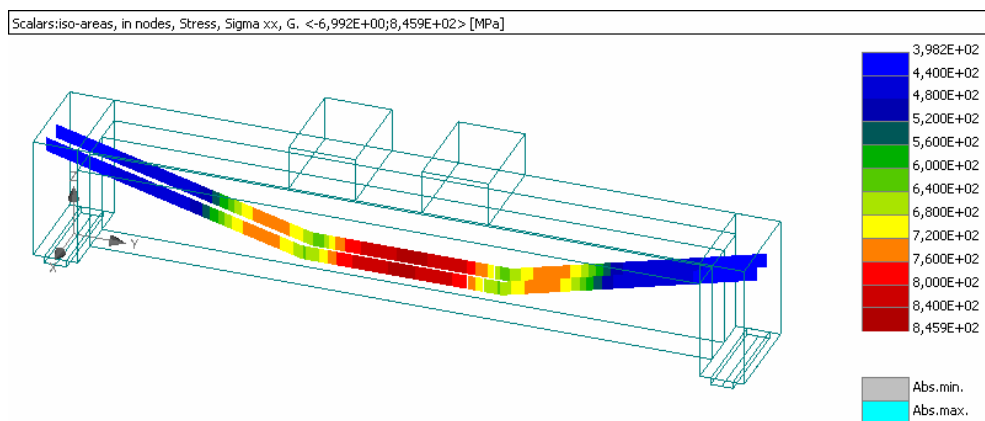


Figure 2-35 Stress distribution in reinforcing bars.

Stress state of the structures illustrated on above figures is in the analysis step 51 under prescribed displacement 4.67mm and load 0.139 MN.

2.8 Beam with external cables (EXTC)

Keywords: reinforced concrete, discrete reinforcement, prestressing by external cables

Input files: EXTC\EXTC.cc2

2.8.1 Introduction

A beam (shown in Figure 2-36) similar to that from the previous example is analyzed. The only difference is in the type of prestressing, which is this time applied by external cables. The cables lack any bond to concrete, except at their anchored ends. The left anchor is active, where the prestressing is applied. The right anchor is passive. The path of the cables is given by two deviators positioned under the load points.

2.8.2 Comments on FE model preparation

2.8.2.1 Materials

The material models are the same as those in example INTB.

2.8.2.2 Topology

The prestressing cable is modeled as a single line consisting of three segments. In addition to the reinforcement topology, it is necessary to prescribe the properties of the deviators. In this analysis, we assume almost frictionless contact between the cables and deviators. The deviators' radii are both identical 25 mm.

2.8.2.3 Loads and supports and Run

As in the previous example, the prestress is applied in the first load step. A prestressing force of 0.2 MN is prescribed in the left cable anchor. The stress due to this force is 410 MPa, which is slightly less than in the previous case of internal cables. Consequently, vertical load is incrementally added by prescribing displacement at the load points.

2.8.3 Results

Selected results are shown in Figure 2-37, Figure 2-38, Figure 2-39 and Figure 2-40. Comparing Figure 2-31 and Figure 2-39 it is seen that the beams with internal and external cables exhibit different cracking behavior. In the former, there is a larger number of finer cracks distributed over the whole beam, while in the latter, cracking is concentrated in the mid-span.

Table 2.8-1 Material properties of concrete

Material type		SBETA material	
Elastic modulus	E_c	33	GPa
Poisson's ratio	ν	0.2	-
Compressive strength	f_c	53.8	MPa
Tensile strength	f_t	3.392	MPa
Type of tension softening		Exponential	
Fracture energy	G_f	183.3	N/m
Crack model		Fixed	

Table 2.8-2 Material properties of prestressing cable

Material type		Reinforcement	
		bilinear	
Elastic modulus	E	200	GPa
Yield strength	σ_y	1600	MPa
Hardening		perfectly plastic	
Total cross-sectional area		$4.9 \cdot 10^{-4}$	m^2
Deviator	Frict. coeff.	0.001	-
	Cohesion	0	MN/m
	Radius	0.025	m

Table 2.8-3 Solution parameters

Solution method	Newton-Raphson	
Stiffness/update	Elastic/each step	
Number of iterations	30	
Error tolerance	0.010	
Line search	on, with iterations	

Table 2.8-4 Finite element mesh

Finite element type	Quadrilateral (CCQ10Sbeta)	
Element shape smoothing	on	
Optimization	Sloan	

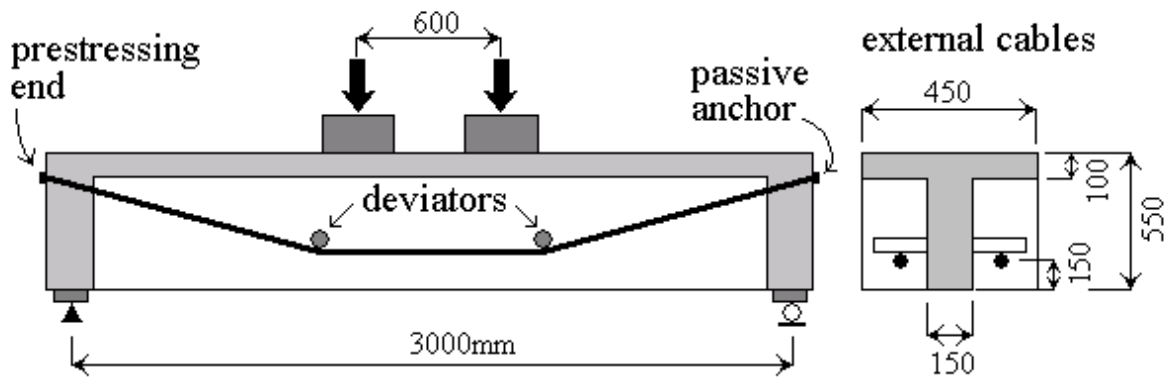


Figure 2-36 Beam prestressed by external cables

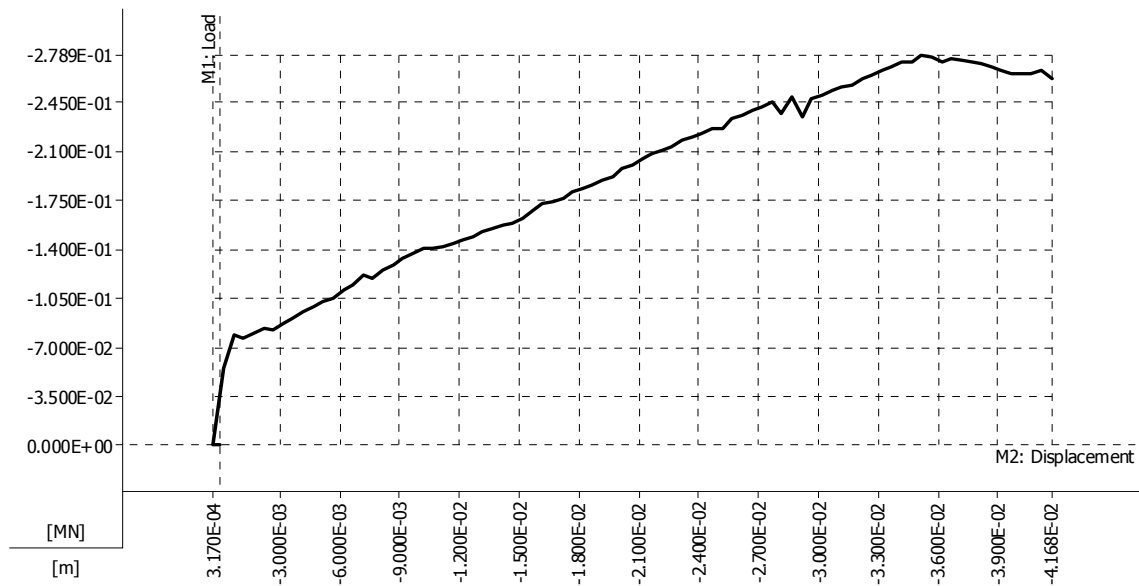


Figure 2-37 Computed load-displacement curve of beam with external cables

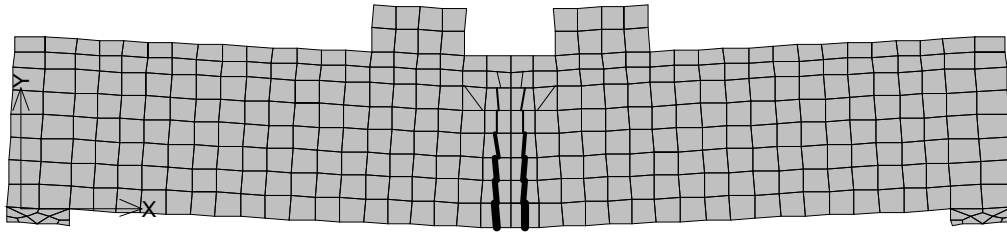


Figure 2-38 Computed crack pattern at load step 12

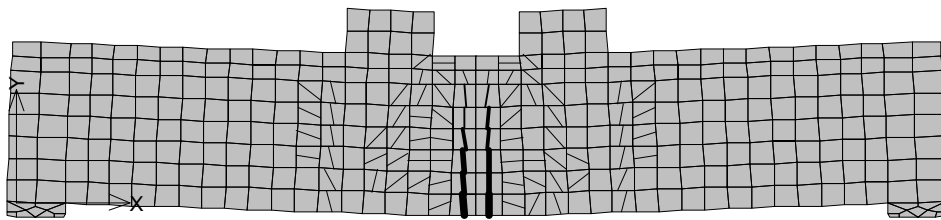


Figure 2-39 Computed crack pattern at load step 82

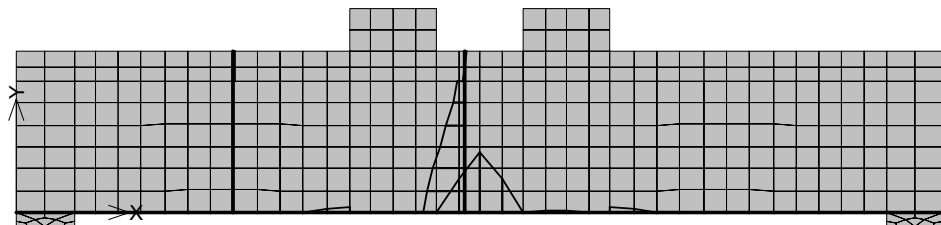


Figure 2-40 Distribution of engineering strain (xx -component) along predefined cut lines at load step 82

2.9 Beam with external cables (EXTC) 3D

Input file: EXTC.cc3

The same girder as in 2D analysis is considered. The difference is in deviators, which are in this case provided by additional concrete blocks as shown in Figure 2-41. Note, that location of bar points (anchors, deviators) need not to coincide with geometrical points (joints) or mesh nodes.

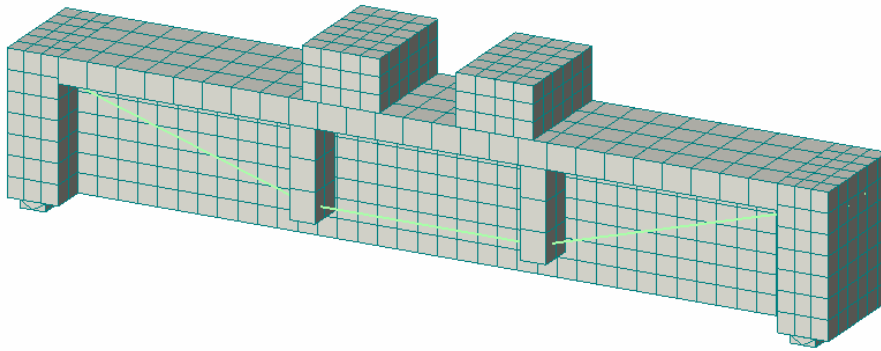


Figure 2-41 Finite element model of beam with external cables.

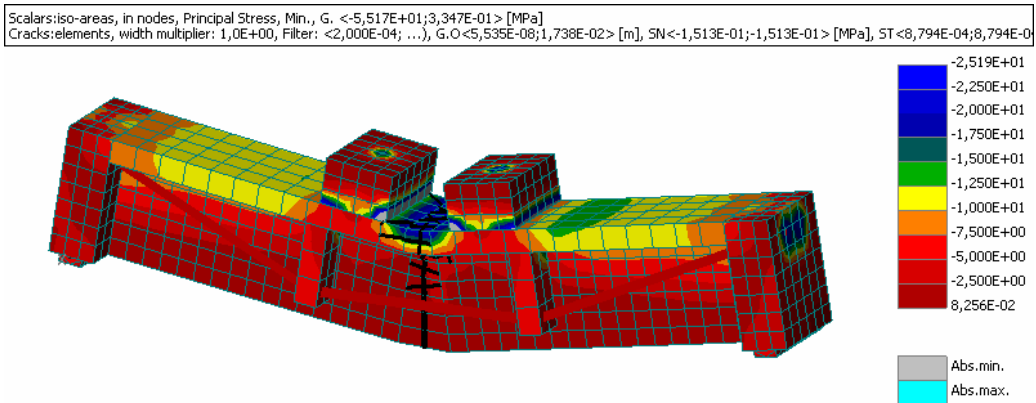


Figure 2-42 Picture of deformation, stress (principal stress min.) and crack state at the load step 41.

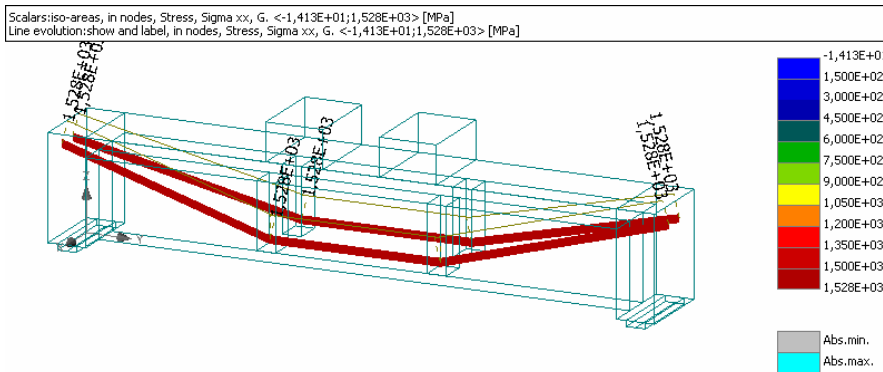


Figure 2-43 Stress distribution in cables at load step 41.

2.10 Shear wall with opening (SWO)

Keywords: reinforced concrete, shear failure, discrete reinforcement, smeared reinforcement

Input files: SWO\SWOL.cc2 (loading from left)
SWO\SWOR.cc2 (loading from right)

2.10.1 Introduction

French institute CEBTP organized a blind test calculation in which a shear wall with opening was loaded by a lateral force [1]. The specimen of a rather complex shape consists of a reinforced concrete panel with an opening. The panel is provided with a top loading beam and a bottom supporting beam. The panel is reinforced by an orthogonal steel mesh in the middle part and by additional stiffening bars along the edges. See **Chyba! Nenalezen zdroj odkazů.**

2.10.2 Comments on FE model preparation

2.10.2.1 General data

If a concrete member is reinforced by a steel mesh, as it is the case in the present example, it is convenient to represent the mesh as smeared reinforcement. In the ATENA program, smeared reinforcement is defined using layers, such that each layer contains only bars having the same direction. The number of these layers must be specified in the “General data” section. Since the panel is reinforced by an orthogonal mesh, the number of layers in this example is two.

2.10.2.2 Materials

The SBETA material model is employed for concrete. Material parameters are listed in Table 2.10-1. Reinforcement is modeled as elastic-plastic material with linear hardening; see Table 2.10-2, Table 2.10-3, Table 2.10-4, and Table 2.10-5. The steel mesh (**Chyba! Nenalezen zdroj odkazů.**) is modeled as smeared reinforcement – horizontal and vertical bars separately. Furthermore, due to having different thickness, the panel and the beams have different reinforcement ratios. To reflect the difference, we define smeared reinforcements in each of the regions as a distinct material. The remaining rods are represented as discrete reinforcement (**Chyba! Nenalezen zdroj odkazů.**).

2.10.2.3 Topology

Despite complexity of the problem geometry, solution is attempted with quite a coarse FE mesh. Element size 0.09 m is prescribed in the panel and bottom beam and 0.0725 m in the upper beam. CCQ10Sbeta elements are used in the panel and the lower beam, while CCIsoQuad elements discretize the upper beam. Discrete reinforcement is modeled by segment lines. The FE model is shown in **Chyba! Nenalezen zdroj odkazů.**

2.10.2.4 Loads and supports and Run

The bottom side of the lower beam is fixed in both horizontal and vertical directions. Loading is applied by prescribing horizontal displacement at the lower corner of the upper beam in constant increments of 0.1 mm. Analysis is performed separately with loading acting from the left side to the right (input file “SWOL.cc2”) and vice versa (input file “SWOR.cc2”). The Newton-Raphson solution method with parameters listed in Table 2.4-3 is employed.

The overall response (horizontal displacement and reaction force) is recorded using two monitoring points – both located in the vicinity of the loading point.

2.10.3 Results

Post-processing of the analytical results revealed that extensive cracking, reinforcement yielding and concrete crushing was taking place in the specimen. Under the left-side loading numerous diagonal cracks formed. The cracking was most intensive near the joint between the lower beam and the panel at the right side. Such a cracking behavior was consistent with that reported in the experiment [1].

The right-side loading resulted in a different cracking pattern. The column on the left side of the opening failed in shear and a large crack propagated diagonally through the panel from the opening to the upper right corner.

The computed overall response of the panel is shown in **Chyba! Nenalezen zdroj odkazů.** for both left-side and right-side loading. The figure also compares the analytical results with the experimental measurements. The analysis predicts well the tendency of the experimental curves up to the peak. However, the analytical results appear to be more brittle after the peak. The real specimen had a more ductile behavior in compression caused probably by a confinement effect of transverse reinforcement. This effect was not considered in the analysis.

2.10.4 References

[1] Foure, B., *Eléments finis appliqués au béton armé ou précontraint (comportement non-linéaire jusqu’à rupture)*, Test de logiciels de calcul, CEBTP (no. 9641006), Février 1998

Table 2.10-1 Material properties of concrete

Material type		SBETA material	
Elastic modulus	E_c	31.7	GPa
Poisson's ratio	ν	0.2	-
Compressive strength	f_c	27.6	MPa
Tensile strength	f_t	2.6	MPa
Type of tension softening		Exponential	
Fracture energy	G_f	100.0	N/m
Crack model		Fixed	

Table 2.10-2 Material properties of mesh reinforcement $\varnothing 6$

Material type		Smeared reinforcement	
		multilinear	
Elastic modulus	E	200	GPa
Yield strength	σ_y	570	MPa
Hardening		linear	

Table 2.10-3 Material properties of reinforcement rod $\varnothing 12$

Material type		Reinforcement	
		multilinear	
Elastic modulus	E	200	GPa
Yield strength	σ_y	480	MPa
Hardening		linear	

Table 2.10-4 Material properties of reinforcement rod $\varnothing 10$

Material type		Reinforcement	
		multilinear	
Elastic modulus	E	200	GPa
Yield strength	σ_y	470	MPa
Hardening		linear	

Table 2.10-5 Material properties of reinforcement rod Ø8

Material type		Reinforcement	
		multilinear	
Elastic modulus	E	200	GPa
Yield strength	σ_y	620	MPa
Hardening		linear	

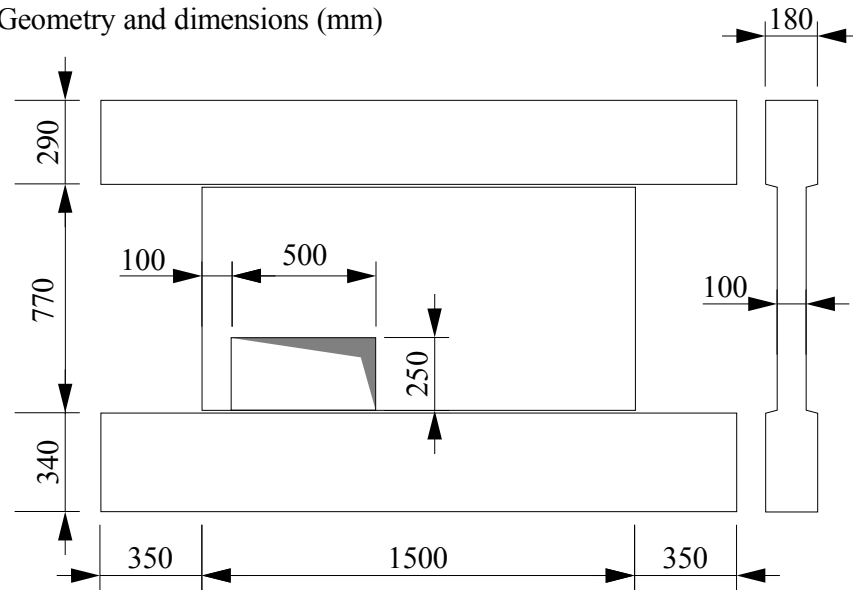
Table 2.10-6 Solution parameters

Solution method	Newton-Raphson	
Stiffness/update	Tangent/each iteration	
Number of iterations	30	
Error tolerance	0.010	
Line search	on, with iterations	

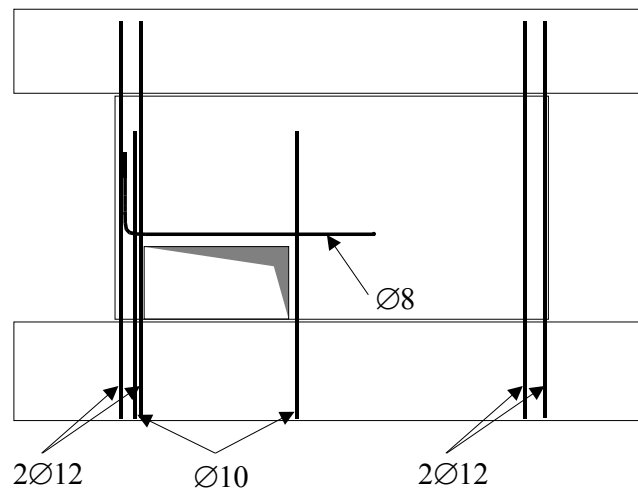
Table 2.10-7 Finite element mesh

Finite element type	Quadrilateral (CCIsoQuad and CCQ10SBeta)	
Element shape smoothing	on	
Optimization	Sloan	

Geometry and dimensions (mm)



Discrete reinforcement



Smearred reinforcement

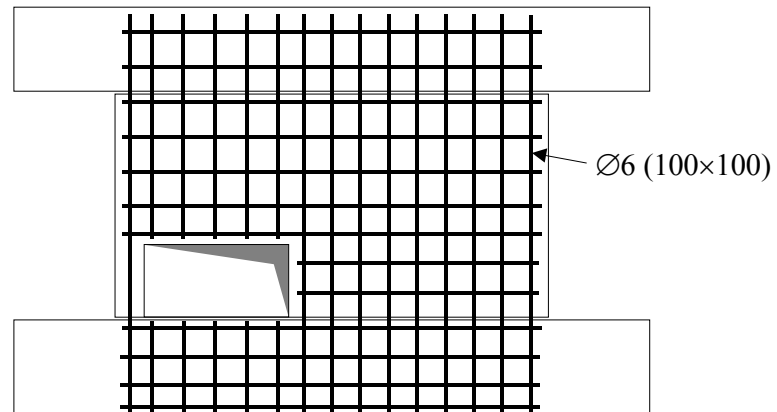


Figure 2-44 Geometry and reinforcement of shear wall

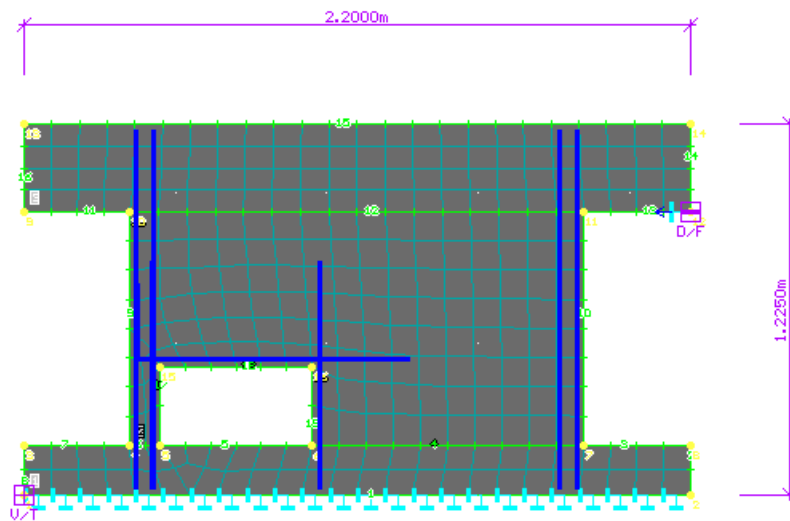


Figure 2-45 FE model of shear wall

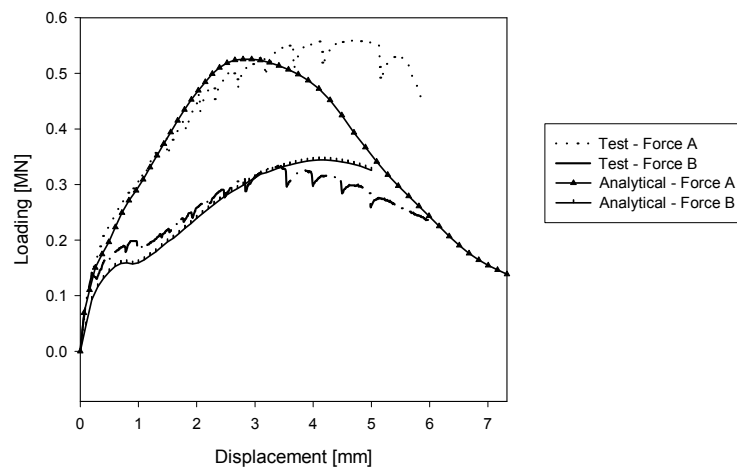


Figure 2-46 Analytical and experimental load-displacement curves of shear wall (A...loading from left, B...loading from right)

2.11 Punching failure of a slab (PUNC)

Keywords: axisymmetry, reinforced concrete, discrete reinforcement, shear failure

Input files: PUNC\PUNC1.cc2

2.11.1 Introduction

In this example we analyze the punching failure of a reinforced concrete slab. The analysis reproduces one of the experiments carried out by Men etrey [1], in which an octagonal RC slab supported by hinges along its circumference was loaded through a short steel column – see Figure 2-47. The slab was very lightly reinforced by steel meshes along its top and bottom surfaces and by a single circumferential rod placed close to the bottom surface. In the experiment, this slab exhibited a typical punching failure, in which shear cracks formed a cone, interior of which was pushed out of the slab by the column. In addition, there were several radial bending cracks. As it is typical for a shear failure, the punching failure was very brittle, with a sharp drop in the load-displacement curve following formation of the conical failure crack.

2.11.2 Comments on FE model preparation

2.11.2.1 General data

The problem is analyzed using the axial symmetry idealization. To this end, it is necessary to select ‘Problem type: Axial symmetry’ in the ‘General data’ window which pops up when creating a new data file.

2.11.2.2 Materials

Concrete is modeled using the 3D Non Linear Cementitious material type with material parameters listed in Table 2.11-1. It should be noticed that for axial symmetry problems it is necessary to input the parameter called ‘Number of radial cracks’, which corresponds to the assumed number of radial cracks that may form in r - z planes. In the present analysis, this number is estimated as 10 from the experimental result.

The circumferential reinforcement is modeled as a discrete ring. Since no cracking is expected near the top surface and the reinforcement ratio of the upper wire mesh is very low, only the lower mesh is modeled. It is approximated by discrete circumferential rods with cross-sectional area corresponding to that of the original mesh rods in one direction. This is a very rough approximation, which should be refined if a more precise analysis is to be carried out. The material of the bars is modeled as elastic perfectly-plastic, with parameters listed in Table 2.11-2 and Table 2.11-3. The loading column is assumed to remain elastic and perfectly bonded to the concrete slab.

2.11.2.3 Topology

Since we solve the problem in axial symmetry, it is necessary to specify topology of the symmetric section only. In order to accurately capture shear cracking, a

relatively fine regular mesh with element size of 1.5 cm is used for the slab. The geometry of the circumferential reinforcement is described by appropriately located points.

2.11.2.4 Loads and supports and Run

The hinge support along the outer circumference, together with the horizontal constraint along the symmetry axis, are prescribed as load case LC1 in all load steps. Loading is applied by prescribing incremental vertical displacement along the symmetry axis at the top of the loading column (LC2). The increment is 0.1 mm for the first 20 load steps and 0.2 mm for the remaining steps.

2.11.3 Results

The computed load-displacement curve is shown in Figure 2-48. Figure 2-49 shows the deformed shape and crack distribution after the load step 20, which just follows the first load drop. The figure reveals a cone formed by inclined shear cracks as well as the radial cracks (denoted by circles).

2.11.4 References

[1] Menétrey, P., Relations between Flexural and Punching Failure, ACI Structural Journal, V.95, No.4, 1998

Table 2.11-1 Material properties of concrete

Material type		3D Non Linear Cementitious	
Elastic modulus	E_c	36.95	GPa
Poisson's ratio	ν	0.2	-
Compressive strength	f_c	42.5	MPa
Tensile strength	f_t	3.257	MPa
Fracture energy	G_f	81.43	N/m
Number of radial cracks		10	-

Table 2.11-2 Material properties of mesh reinforcement

Material type		Reinforcement bilinear	
Elastic modulus	E	210	GPa
Yield strength	σ_y	640	MPa
Hardening		perfectly plastic	

Table 2.11-3 Material properties of circumferential reinforcement

Material type		Reinforcement bilinear	
Elastic modulus	E	210	GPa
Yield strength	σ_y	621	MPa
Hardening		perfectly plastic	

Table 2.11-4 Solution parameters

Solution method	Newton-Raphson	
Stiffness/update	Elastic/each step	
Number of iterations	20	
Error tolerance	0.01/0.02/0.05/0.01	
Line search	on, with iterations	

Table 2.11-5 Finite element mesh

Finite element type	Quadrilateral	
Element shape smoothing	on	
Optimization	Sloan	

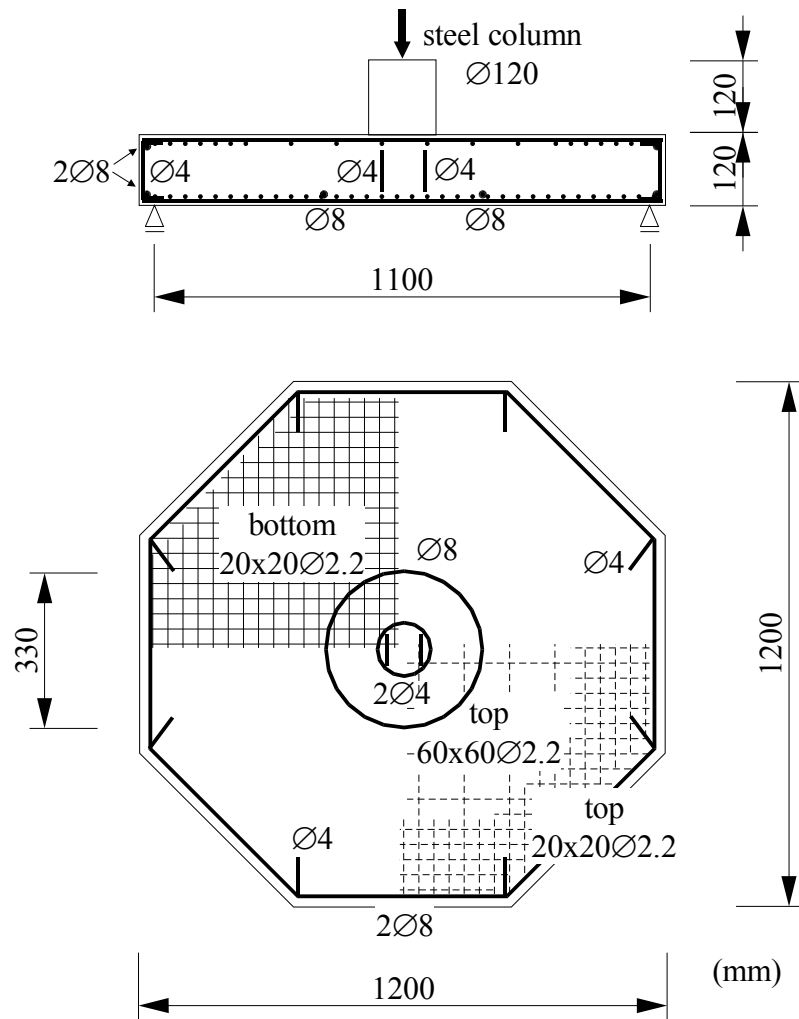


Figure 2-47 Arrangement of the slab punching experiment and the slab geometry and reinforcement

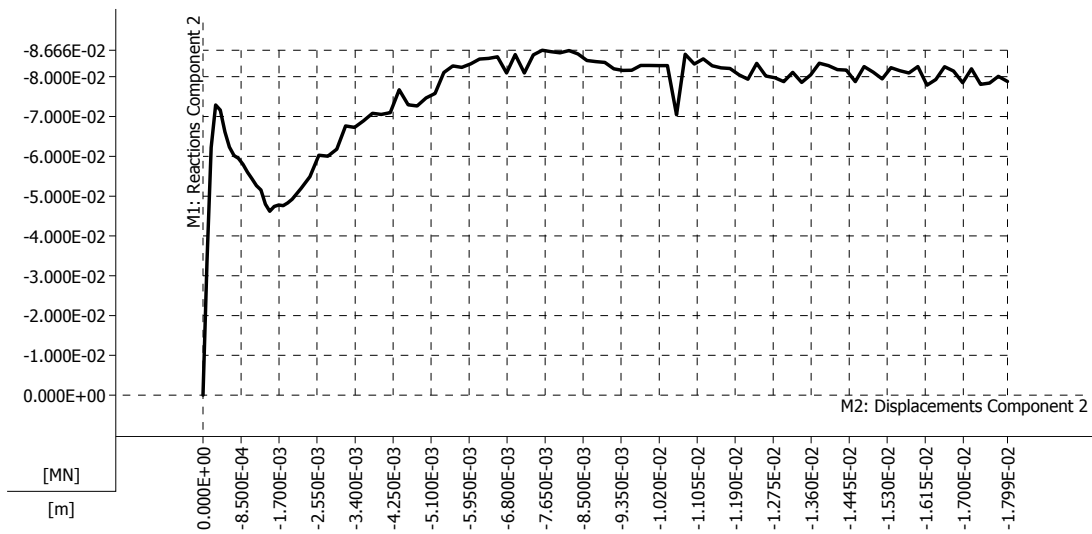


Figure 2-48 Computed load-displacement curve of the axisymmetric slab

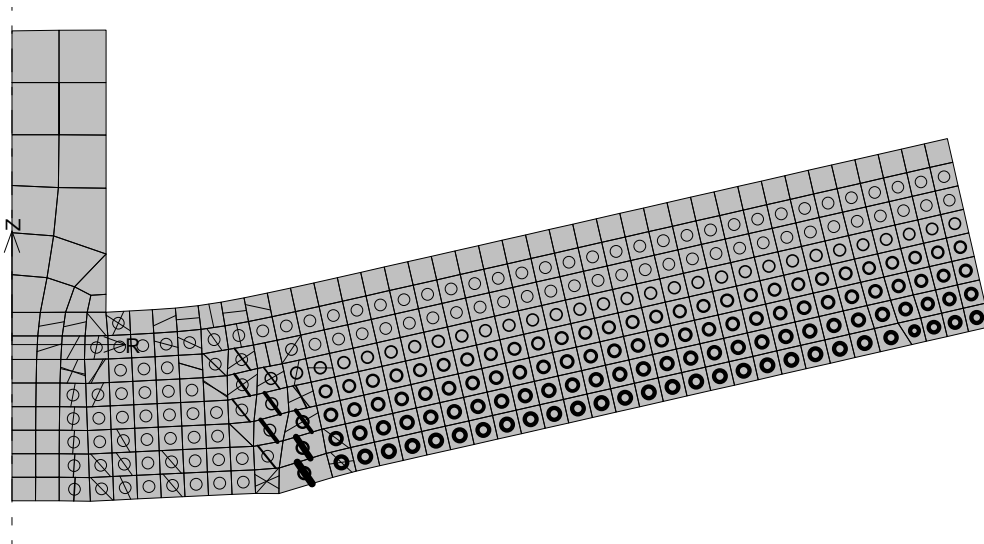


Figure 2-49 Computed deformed shape and crack distribution after load step 20

2.12 Bond failure (BOND)

Keywords: reinforced concrete, discrete reinforcement, bond failure

Input files: BOND\BOND_BIGAJ.cc2, BOND_CYCLIC.cc2

2.12.1 Introduction

This example demonstrates the bond behavior of anchoring bars in the wall-plate joint. The anchoring length of the bars under observation is deliberately short so that a bond slip can be induced. Other reinforcement is strong enough to prevent other modes of failure. The purpose of this example is to show the features of two bond models: Bond model by Bigaj under a monotonic loading and the plastic bond law under a cyclic loading. The example should not be considered as properly designed under normal circumstances.

2.12.2 Comments on FE model preparation

General data

The problem is modeled using the plane stress idealization. Thus after starting ATENA 2D environment it is necessary to select the menu item **File | New | Problem type: 2D**.

Materials

Concrete is modeled using the Sbeta Material, (damage-based concrete constitutive model for plane stress). The vertical part (-wall) is made of concrete 40 and the base slab of concrete 30. Reinforcement bars are using the bi-linear, elastic-plastic stress strain law.

We consider two types of bond properties: poor bond by Bigaj [1] and user defined perfectly-plastic bond slip. The bond slip laws are shown in Figure 2-51.

The bond properties can be defined in the menu **Materials | New material | Reinforcement Bond**. In this menu the bond law according to Bigaj is a pre-defined option and can be simply selected. The perfectly plastic bond law we define by using user option available in this menu. Here we enter the law by specifying the maximal bond stress 4.9 MPa for the starting point (slip 0.0) and the end point (slip 0.0049 m).

Interface line between the wall and the base plate represents a joint with no tensile strength. It is modeled by the interface material with no tensile strength but some cohesion in shear.

We solve two cases with different shapes of bond law and the same maximal bond stress. Other properties of both cases are identical.

Material properties used in this example are listed in Table 2.12-1, Table 2.12-2, Table 2.12-3.

Topology and loading

The structure is a detail of a wall-base plate corner. The model represents a symmetrical half of a U-shaped structure, with the vertical line of symmetry on the right edge of the base plate. The horizontal loading is applied 0.1 m below the wall top edge in form of prescribed displacement. Horizontal reaction force is then calculated as a response to the applied displacement.

Only discrete bars are used for the reinforcement. The bar reinforcement no.2 consisting of 2 bars of profile 12mm are connecting the wall with the base plate. The transmission of tensile forces from the wall to the base plate is assured only by bond between steel bars and concrete. The anchoring length of the vertical bars (reinforcement no.2) in the base plate was made deliberately short (0.2 m) in order to demonstrate the bond failure.

The geometry and material properties of the bars can be entered first. Then only for the bars, which should include a bond slip option, an appropriate bond model (previously defined in materials) can be assigned. This is done in the dialog box for input of reinforcement bars **Edit reinforcement bars | Properties | Reinforcement Bond | Connection to the material | Bond model** . (Of course the same can be done when creating the **Reinforcement bar prototype**, or **New reinforcement bars**.) In this dialog window we must first enter the perimeter of reinforcement. This is in our case (see topology below) a total perimeter of 2 bars no.12, which is 0.0754 m. Then we can select one of the pre-defined bond materials.

Only the bars in the reinforcement no.2 will be modeled with bond. Other reinforcement is without bond model (option **perfect connection**).

Load cases

Two load cases are defined: (1) Supports, (2) Prescribed displacements.

In the load case 1 horizontal support is prescribed on the line of the symmetry in the base plate (right vertical edge). Vertical support in the joint 6 is needed to complete a stable support condition (structure does not slide vertically).

Load case 2 prescribes a horizontal displacement -0.0001m in the joint 10.

Monitoring points, solution method

Monitoring points are chosen in order to describe a load-displacement response. Compact Reaction is monitored at joint 10 (point of load application). Horizontal displacement is monitored at the same location. Note that multipliers -1000 have been used for monitoring in order to get the response in a convenient format (positive numbers, mm, kN).

Solution method

Solution method is chosen as slight modification of the Standard Solution Method. In this method the number of iterations was increased to 100. The reason for this is expected slower convergence of the bond element. The method is stored under the name "NR 100". The convergence limit for residual forces was chosen 0.001 for the case BOND_BIGAJ and 0.01 for the case BOND_CYCLIC.

Analysis steps

Bond by Bigaj:

Load steps include: load cases 1 and 2, solution method NR100. Load history is composed of the 20 load steps with the coefficient 1.0 followed by 25 load steps with the coefficient 5.0.

Bond cyclic:

In this case a cyclic loading induced by imposed displacement is applied as follows:

Loading in 10 steps up to the displacement 1.0 mm.

Unloading in 4 steps down to the displacement 0.6 mm.

Reloading in 7 steps up to the displacement 1.3 mm.

Unloading in 4 steps down to the displacement 0.9 mm.

Reloading in 7 steps up to the displacement 1.6 mm.

Run

Analysis can be started by pressing the button **Run finite element analysis**. Response can be observed during the solution by activating the monitoring points (displacement on X, reaction on Y) and by choosing some option of the analysis progress monitoring (after load step, etc.). In this way we can run both cases for two different bond models.

2.12.3 Results

Behavior of the structure is strongly affected by anchoring of the vertical bar. The horizontal force induces a moment in the wall base, which is resisted by two forces, compression in the contact of wall and base and tension in the bar crossing the contact joint. The joint opens immediately after the loading and no tension in the interface exists. The tension in the bar is transferred to the base by the bond stresses only.

The computed load-displacement curve can be displayed using the **Graph** option. It can be also shown using Excel graphic. (The data can be transported to Excel using the **Text printout** option. Select **Results | Monitoring points after load steps** and **Generate**. After this a text file with a list of monitored values will be created. This list can be transferred to the Excel sheet by the copy/paste method.) The load-displacement diagram reflects closely the bond-slip law. Distribution of bond stresses and opening of the interface contact in various load stages is shown in enclosed figures. Variety of other results can be presented graphically: Bond slip, stress in the bar, etc.

The cyclic response is shown in Figure 2-56. The changes of the bond stress distribution under load reversal can be seen in enclosed figures.

Comment on bond model by Bigaj

The brittle behavior of the Bigaj's model is attributed to the splitting mode of bond behavior and is more realistic than the plastic behavior. The present bond model in ATENA is not directly dependent on confinement caused by the normal stresses acting on planes parallel with the reinforcement direction. However, this effect can be to a certain extent furnished by user, when choosing appropriate bond law. For this reason the bond law by Bigaj has three forms according to the confinement: poor, good, very good.

Note that the load-displacement curve does not go to zero at the end. This is caused by the other vertical reinforcement located near the compression corner (left). This

reinforcement is activated in the late load stage and provides some residual resisting capacity.

In this example no cracks occur in most of the loading history. This is due to low stresses in concrete. However, a bond behavior in a cracked concrete functions in a similar way. It should be realized, that in most practical cases the bond is not a significant effect because the bond strength is only seldom reached.

Comment on the plastic model

The plastic bond model is simple, but can serve as a good approximation. The example shows that it can capture the plastic bond slip also for a cyclic loading.

Convergence limits

Note that two convergence limits has been used in these examples and both give satisfactory results. The limit 0.01 converges in about 10 iterations, while the limit 0.001 in about 20 iterations. The higher limit gives more precise results, but the difference is not significant.

2.12.4 References

[1] Bigaj, A.J. – Structural Dependence of Rotation Capacity of Plastic Hinges in RC Beams and Slabs. PhD Thesis, Delft University of Technology, 1999. ISBN 90-40-1926-8.

Table 2.12-1 Material properties of concrete

Material type		Sbeta C30 Base	Sbeta C40 Wall
Elastic modulus	GPa	E_c	30.32
Poisson's ratio -		ν	0.2
Compressive strength	MPa	f_c	25.5
Tensile strength	MPa	f_t	2.32
Fracture energy	N/m	G_f	58
Compressive plast. def.	m	w_d	-0,05

Table 2.12-2 Material properties of reinforcement

Material type		Reinforcement	
		bilinear	
Elastic modulus		E	210 GPa
Yield strength		σ_y	700 MPa
Hardening		perfectly plastic	

Table 2.12-3 Material properties of bond

Material type		User	Poor bond by Bigaj
Function		constant	multi-linear with softening
Max. bond stress [MPa]	$\tau_{b,max}$	4.9	4.9

Table 2.12-4 Material properties of interface

Material type		2D Interface
Normal stiffness K_{nn}	MN/m ³	200 000
Tangential stiffness K_{tt}	MN/m ³	200 000
Normal stiffness minimal K_{nn}^{MIN}	MN/m ³	200
Tangential stiffness minimal K_{tt}^{MIN}	MN/m ³	200
Tensile strength f_t	MPa	0.0
Cohesion C	MPa	2.0
Friction coefficient ϕ	-	0.2

Table 2.12-5 Finite element mesh

Finite element type	CCIsoQuad – Quadrilateral, isoparametric
Element shape smoothing	on
Optimization	Sloan

Table 2.12-6 Solution parameters

Solution method		Newton-Raphson	
Stiffness/update		Tangent/each iteration	
Number of iterations		100	
Error tolerance	Bond by Bigaj Cyclic	0.01/0.001/0.01/0.01 0.01/ 0.01/0.01/0.01	
Line search		on, with iterations	

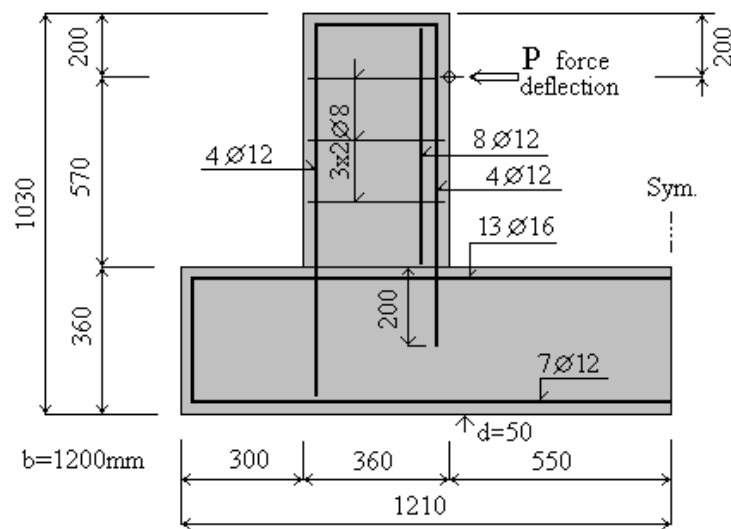


Figure 2-50 Geometry of bond test.

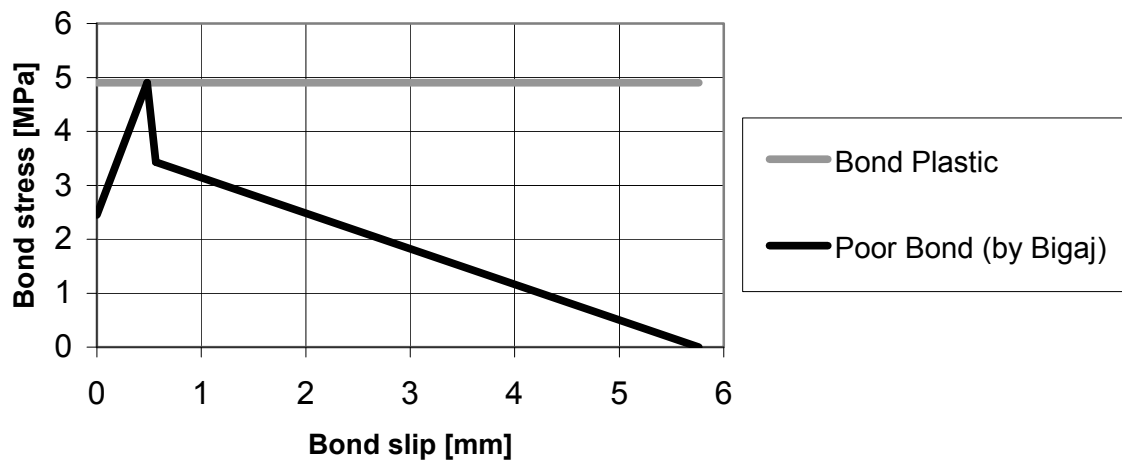


Figure 2-51 Bond-slip laws.

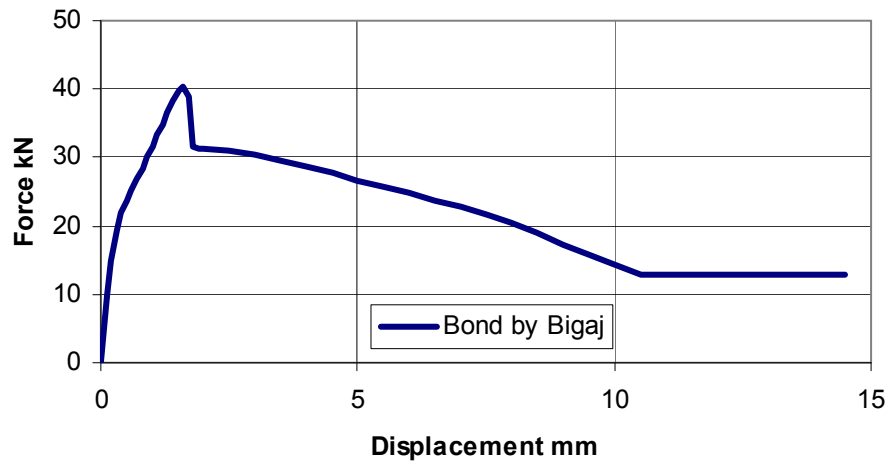


Figure 2-52 Load-displacement diagram of Bond by Bigaj. Horizontal displacement and load applied at the top of wall, see Figure 2-50.

Step 1, Bond by Bigaj
Reinforcements: Bond Stress, Stress(m), <-2.489E+00;2.489E+00>[MPa]

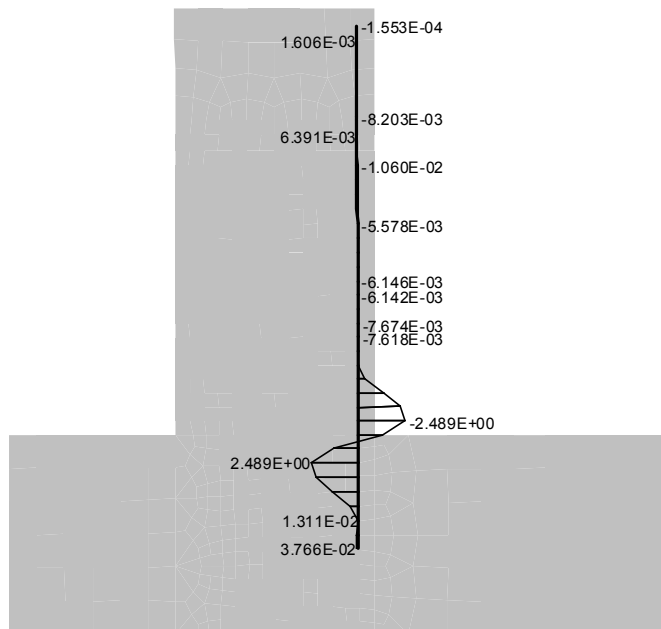


Figure 2-53 Bond stress in the vertical bar at $d=0.1\text{mm}$, LS 1.

Step 16, Bond by Bigaj
 Reinforcements: Bond Stress, Stress(m), <-3.213E+00;4.787E+00>[MPa]

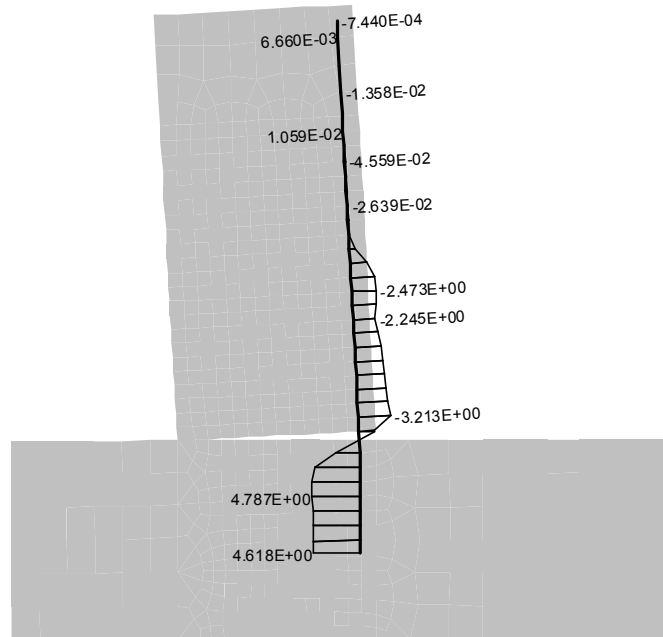


Figure 2-54 Bond stress in the vertical bar at $d=1.6\text{mm}$, LS 16. Displacements enlarged by factor 10.

Step 40, Bond by Bigaj
 Reinforcements: Bond Stress, Stress(m), <-2.521E+00;2.906E+00>[MPa]

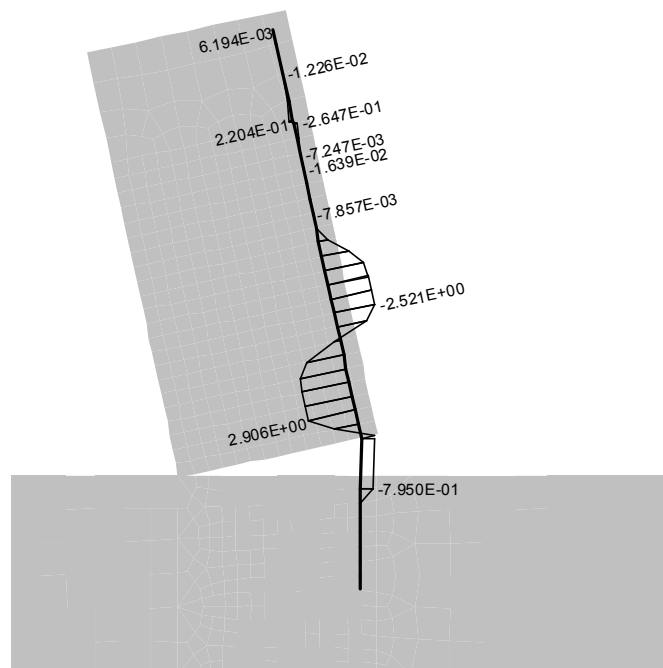


Figure 2-55 Bond stress in the vertical bar at $d=4\text{ mm}$, LS 40.

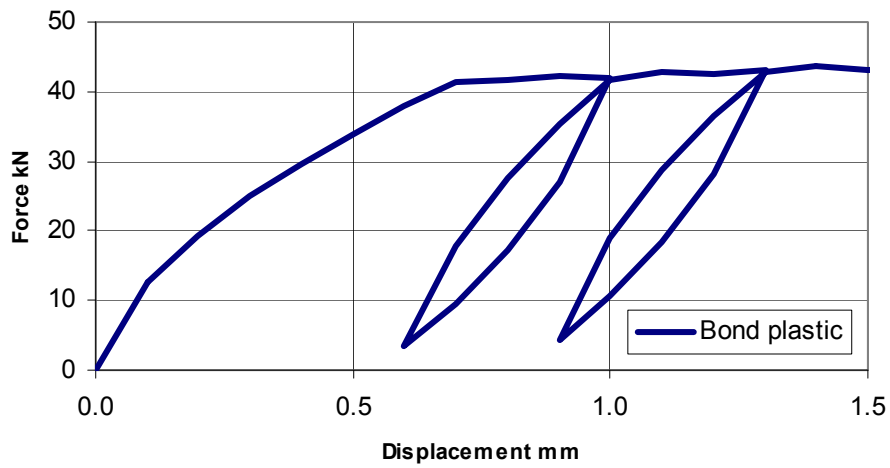


Figure 2-56 Load-displacement diagram of the plastic bond under the cyclic load history. Horizontal displacement and load applied at the top of wall, see Figure 2-50.

Step 10, Bond Cyclic
Reinforcements: Bond Stress, Stress(m), <-4.899E+00;4.900E+00>[MPa]

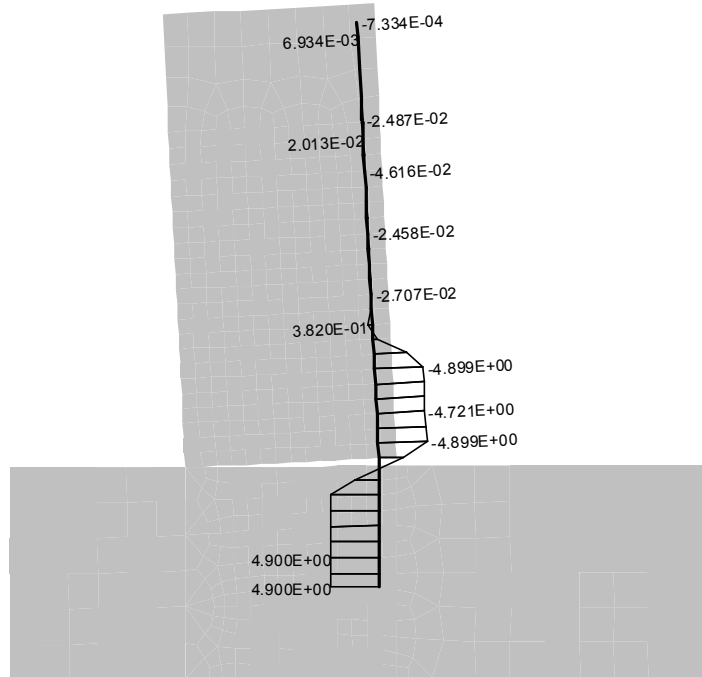


Figure 2-57 Bond stress in the vertical bar at $d=1$ mm, LS 10, loading. Displacements enlarged by factor 30.

Step 14, Bond Cyclic
Reinforcements: Bond Stress, Stress(m), <-4.901E+00;4.901E+00>[MPa]

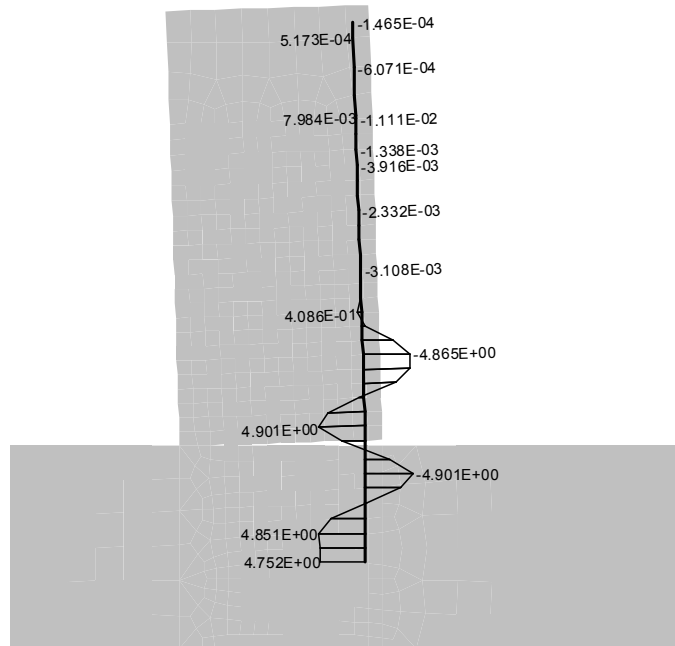


Figure 2-58 Bond stress in the vertical bar at $d=0.6$ mm, LS 14, unloading. Displacements enlarged by factor 30.

Step 21, Bond Cyclic
Reinforcements: Bond Stress, Stress(m), <-4.917E+00;5.085E+00>[MPa]

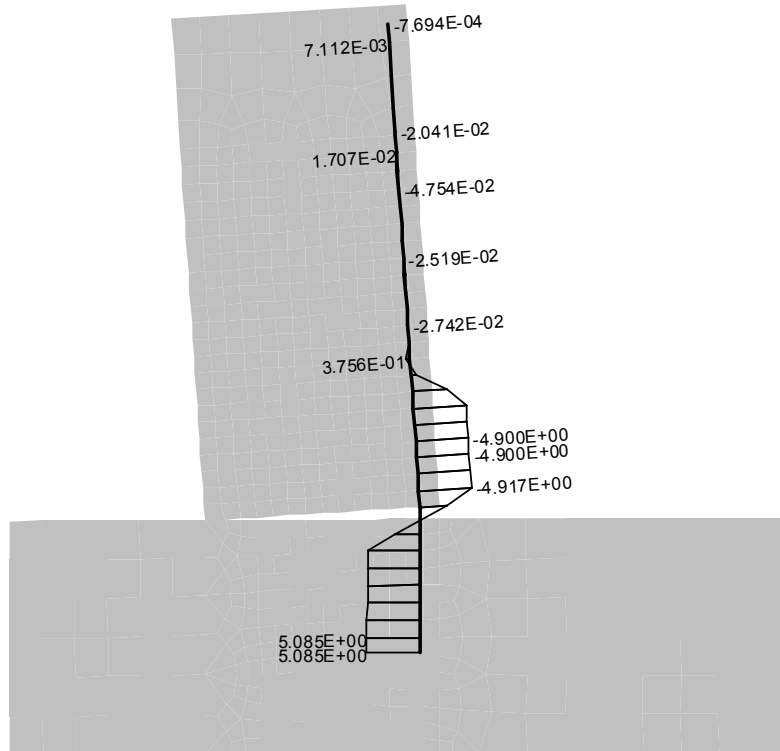


Figure 2-59 Bond stress in the vertical bar at $d=1.3$ mm, LS 21 reloading.

2.13 Construction process of two-layer plate, 3D

Input files:

Slab_brick.cc3 - Two plates, brick elements.

Slab_shell.cc3 - Two plates, shell elements.

2.13.1 Model description

The layered plate structure is constructed and loaded in two phases. The analysis take into account the construction process in which the geometry and loading may change during analysis. The dimensions of plate is shown in .

Construction cases:

- (1) The bottom plate, span 2m, width 1m and thickness 0,2 m is reinforced by 10 ϕ 20mm near the bottom face. It is simply supported and loaded on the top surface by uniform loading 0,06 MN/m². The loading represent the pressure of concrete cast on the top surface, while the bottom plate serve as a form to the top plate. Construction case 1 is applied in four load steps.
- (2) The top plate of the same plane dimensions is cast on top of the bottom plate. Its thickness is 0,3m. After hardening of the top plate it is loaded on the top surface by uniformly distributed load 0,15 MN/ m². Construction case 2 is applied in three load steps.

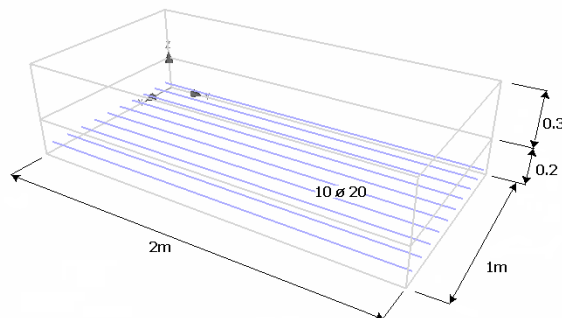


Figure 2-60 Dimensions of layered plate structure.

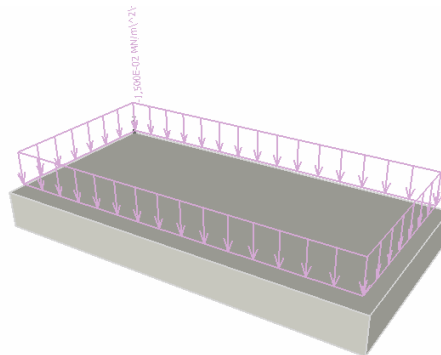


Figure 2-61 Construction case 1.

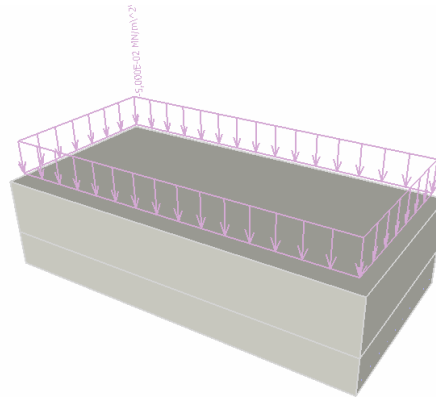


Figure 2-62 Construction case 2.

Hints for FE model:

- (1) First we define materials and construction cases 1 and 2.
- (2) Both plate layers are generated using “Macroelement | Add” tools in a standard way. Bottom plate is provided by discrete reinforcing bars. One bar can be generated by numerical input of end coordinates. Then, remaining bars can be quickly generated by “Copy” command. The construction process is taken into account by assigning the objects to appropriate construction cases: Bottom plate and reinforcing is in the construction cases 1 and 2. Top plate in construction case 2 only.
- (3) Loading is applied. It is associated with geometrical object and automatically assigned to construction cases chosen for objects. It is important that the surface loading is applied to appropriate objects. This must be carefully selected at the top surface of the bottom plate. This location is a contact plane between two macroelements and there are two surfaces on the same location. It is important, that the top surface of the bottom plate (surface 6 of macroelement 1) is loaded. (Not the bottom surface of top plate, surface 5 of macroelement 2).

Materials: For concrete is used material 3D Nonlinear Cementitious 2 with cube $f_{cu}=30\text{Mpa}$. In case of shell element tension parameters modified by setting crack spacing 0.05m and tension stiffening 0.4. Reinforcement is bilinear.

2.13.2 Results – brick model

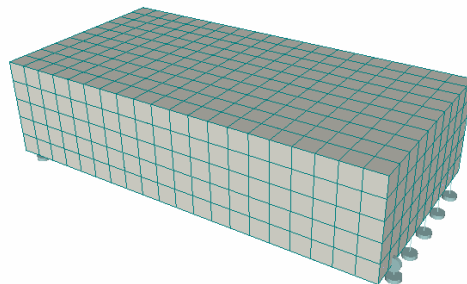


Figure 2-63 Finite element model – brick elements.

In this case plates are modeled as 3D solids by brick isoparametric finite elements, Figure 2-63. Stress iso-areas, cracks and deformations are shown for two construction cases in Figure 2-64 and Figure 2-65. It is interesting to note the technique of connection between old and new object (between construction cases 1 and 2). The mesh of new object – top plate, is on the contact plane adjusted to deformed mesh of existing macroelements. On the contact plane only, the geometry of the added object is adjusted to the deformed shape of the existing object. This can be seen in Figure 2-65. This method corresponds to a casting of added objects on deformed shape of existing objects.

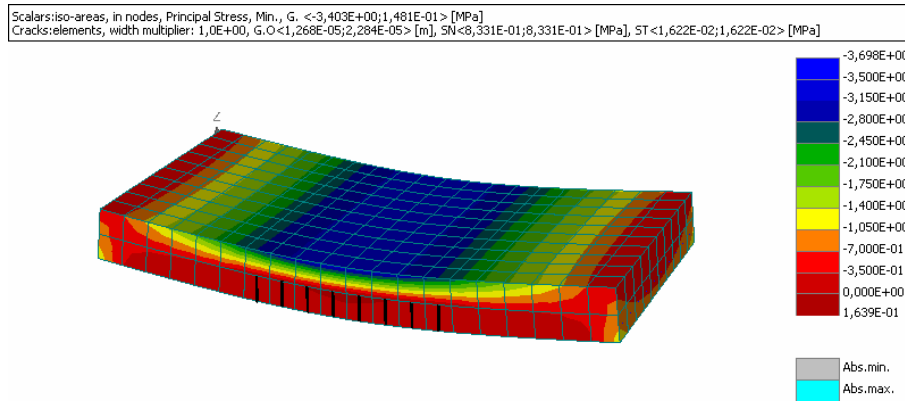


Figure 2-64 Stress, cracks and deformation after construction case 1 – load step 4.

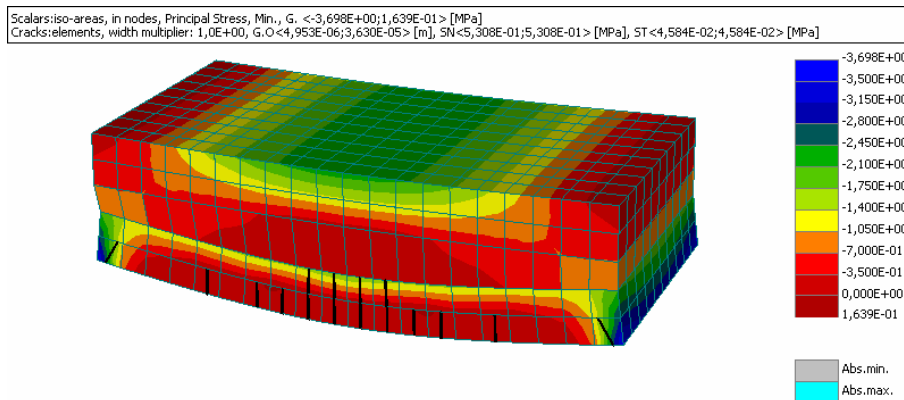


Figure 2-65 Stress, cracks and deformation after construction case 2 – load step 7.

2.13.3 Results - shell model

Alternatively, the same model can be performed using shell elements, which are very efficient for bending-type of behavior. In this case each layer is modeled as a shell object and relatively large elements are chosen, with element size of 0.5m.

The comparison of two types of models and different element sizes is shown in the table below. The results show, that the coarse shell model (element size 0,5m) gives useful result, with an over-estimation of stress and deflection. This is of course on safe side. The elapsed times of calculation show that shell elements are much more time effective. The above pictures show only the results of cases with coarse mesh. Analyses with alternative meshes can be done by modifying “global element size” in the menu “FE mesh | Generation”.

Summary of results and computer time for construction process analysis.

<i>model</i>	<i>element size [m]</i>	<i>no. of finite elements</i>	<i>deflection at midspan [mm]</i>	<i>stress in top at midspan [Mpa]</i>	<i>crack width [mm]</i>	<i>computer time [min]</i>
bricks	0.10	1000	1.04	-2.45	0.04	11.4
bricks	0.05	8000	1.14	-2.81	0.06	149.0
shell	0,50	16	0.99	-2.9	0,015	0.9
shell	0.25	64	0.987	-2.7	0,08	2.6

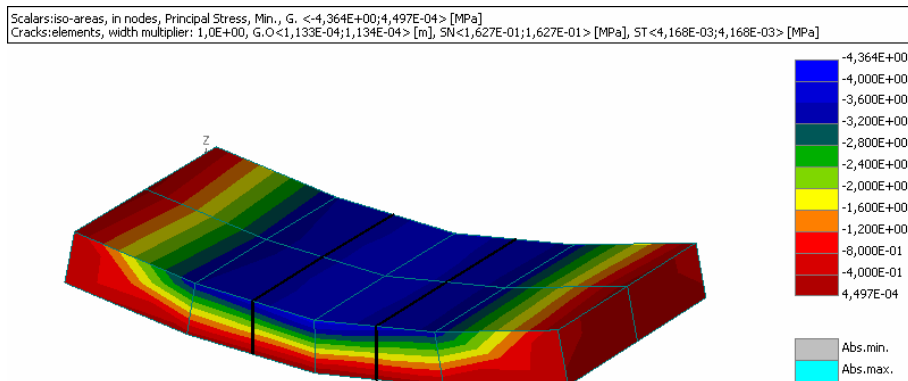


Figure 2-66 Shell model. Stress, cracks and deformation after construction case 1 – load step 4.

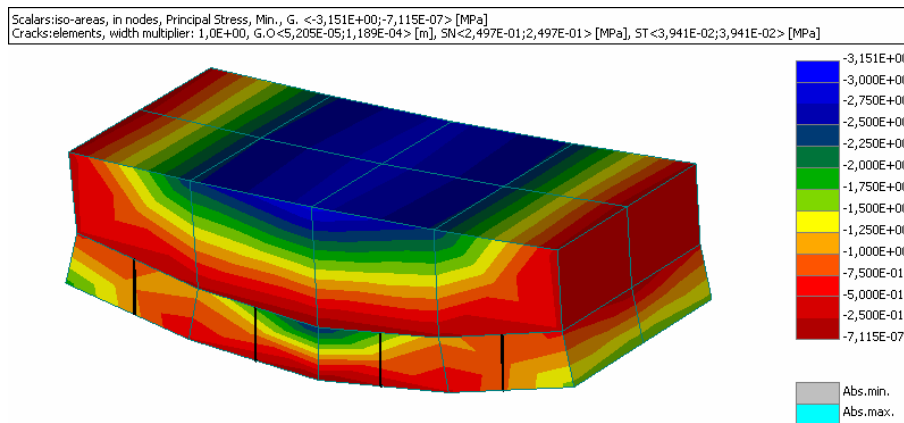


Figure 2-67 Shell model. Stress, cracks and deformation after construction case 2 – load step 7.

3 MESH STUDY

3.1 Comparison of 2D, shell and 3D beam elements

3.1.1 Model description

Cantilever beam with known engineering solution (Bernoulli hypothesis) is the subject of this study. The beam is modeled by different types of elements and meshes.

Following ATENA elements are considered in this study:

- Plane stress 2D isoparametric 8 node low order element (CCIsoQuad),
- Shell Ahmad high order layered element (Shell/Plate),
- Beam 3D high order fiber element (3D Beam).

Mesh of 2D beam and shell elements are shown in Fig. The 3D beam element mesh is identical with the shell, whereas the only difference is in the system of integration by layers in shell and fibers in 3D beam.

Structure: cantilever fixed at one end, length $L=1\text{m}$, width $b=1\text{m}$, thickness $h=0.1\text{m}$.

Loading by distributed forces on the top surface $p=0.1\text{MN/m}^2$

Material elastic: $E=30000\text{ MN/m}^2$, $\mu=0.2$

Solution according to Bernoulli hypothesis:

$$M= L^2 0.5 p = 0.05\text{ MNm}$$

$$W= b h^2/6=0.00166667\text{ m}^3$$

$$J= b h^3 /12 = 0.8333333\times 10^{-5}\text{ m}^4$$

$$\text{Stress at the fixed end, top surface} \quad \sigma = \frac{M}{W} = \frac{0.05}{0.001666} = 30\text{ MPa}$$

$$\text{Tip deflection} \quad y = \frac{QL^3}{8EJ} = \frac{0.1}{8 \times 0.3 \times 10^5 \times 0.833333 \times 10^{-5}} = 0.005\text{ m} = 5\text{ mm}$$

3.1.2 Results

Results are summarized in the following tables.

Plane stress, isoparametric low order rectangular element

Elements through the thickness	Element size m	Tip deflection mm	Stress at fixed end, top edge MPa
10	0.01	5.024	29.59
5	0.02	4.954	25.90
2	0.05	4.522	17.39
1	0.1	3.47	6.47

Shell element

Layers through thickness	Element size m	Tip deflection mm	Stress at fixed end, top edge MPa
10	0.2	4.970	31.63
10	0.5	4.960	31.00
4	0.2	5.253	33.40
2	0.2	6.490	41.57
2	0.1	6.497	41.71

Beam element

Fibers through the thickness	Fibers through the width	Element size m	Tip deflection mm	Stress at fixed end, top MPa
10	10	0.2	4.893	28.77
10	10	0.5	4.638	21.44

Summary of FE models

Model	Number of elements	Number of DOF
2D size 0.01m	1000	2222
2D size 0.05m	40	126
Shell size 0.2m	25	496
Shell size 0.5m	4	97
3D beam size 0.2m	5	60
3D beam size 0.5m	2	24

Following figures illustrate the mesh models and results.

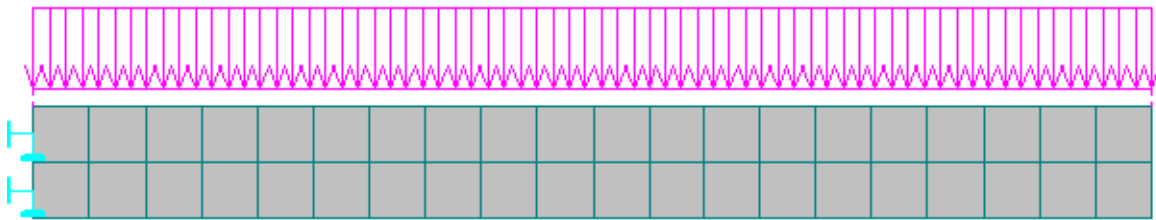


Figure 3-1 2D plane stress elements. Coarse mesh with 2 elements through thickness, element size 0.05 m. Distributed load shown on the top surface.

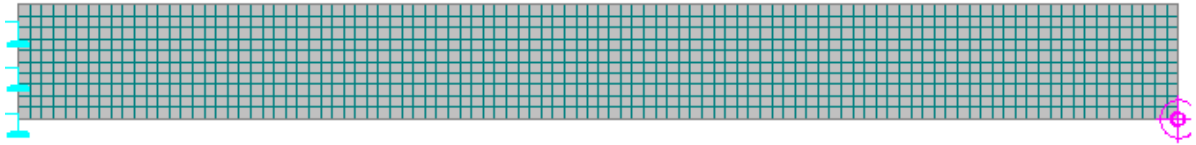


Figure 3-2 2D plane stress elements. Fine mesh with 10 elements through thickness, element size 0.01 m.

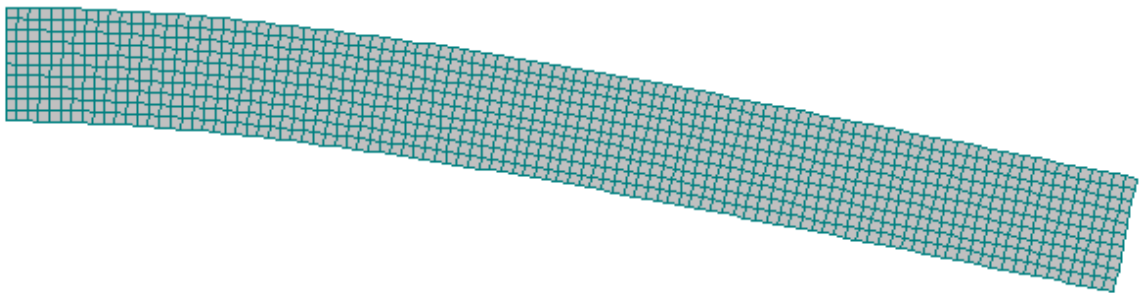


Figure 3-3 2D plane stress elements. Fine mesh with 10 elements through thickness, element size 0.01 m. Deformed form.

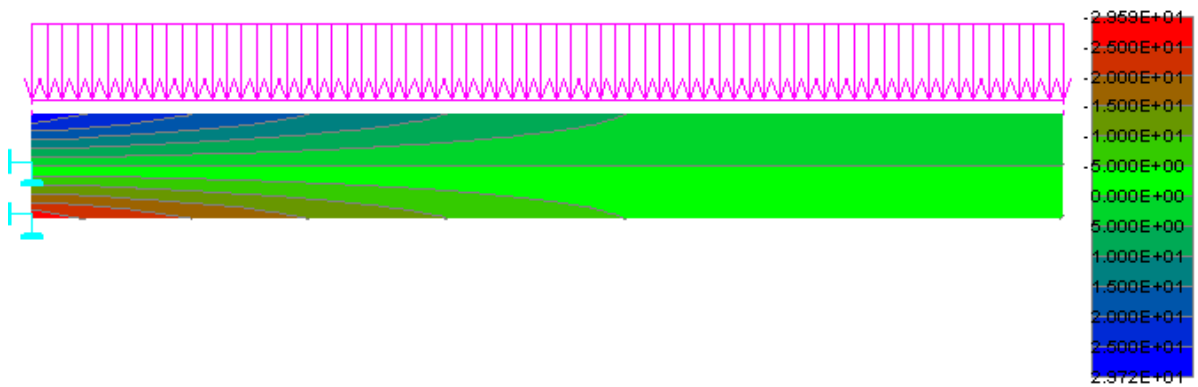


Figure 3-4 2D plane stress elements. Fine mesh with 10 elements through thickness, element size 0.01 m. Iso-areas of axial stress (horizontal).

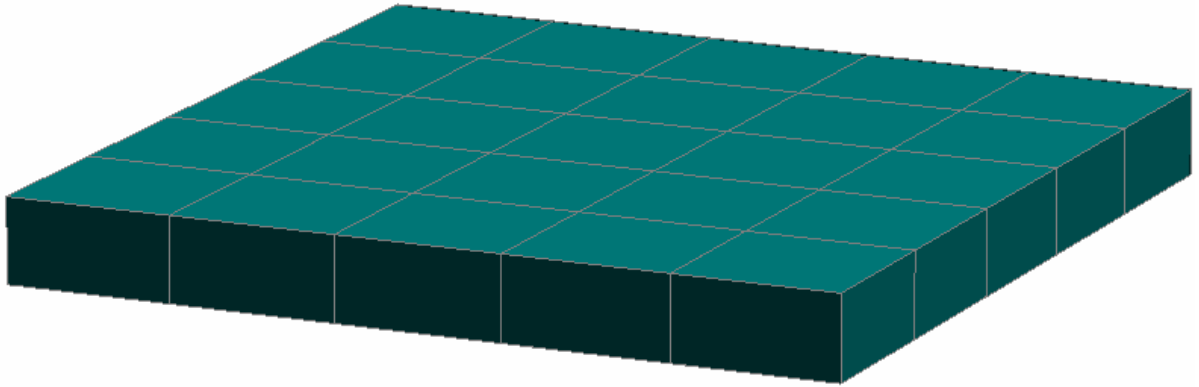


Figure 3-5 Layered shell elements. Mesh model with element size 0.2m.

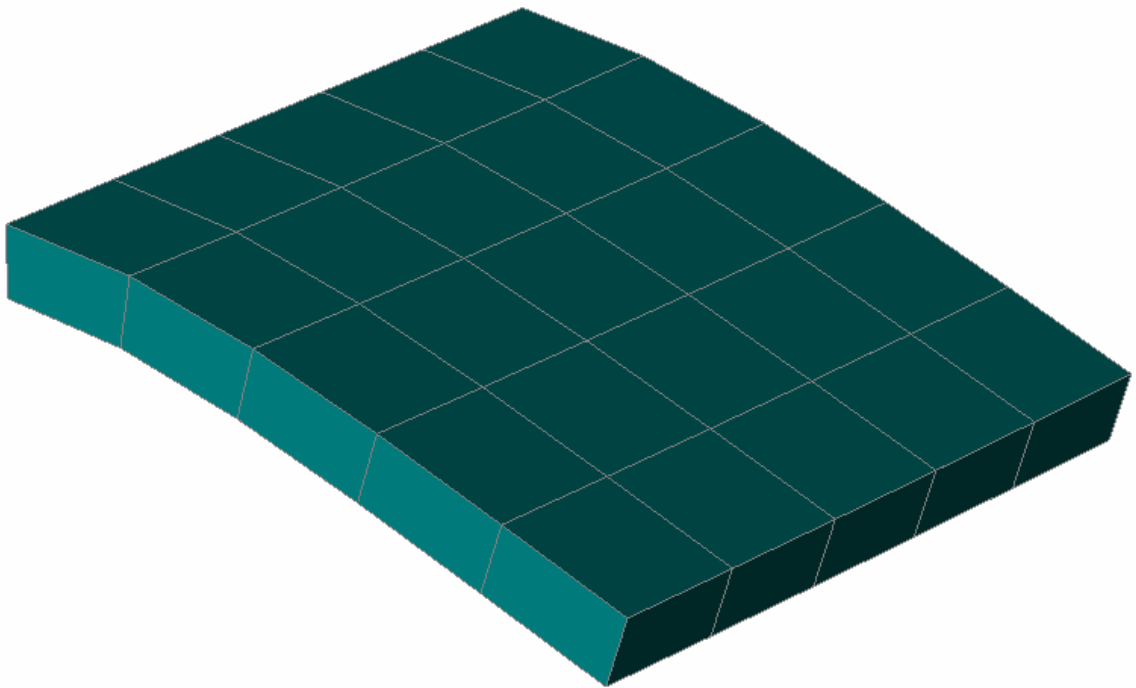


Figure 3-6 Shell elements. Mesh model with element size 0.2m, 10 layers. Deformed form.

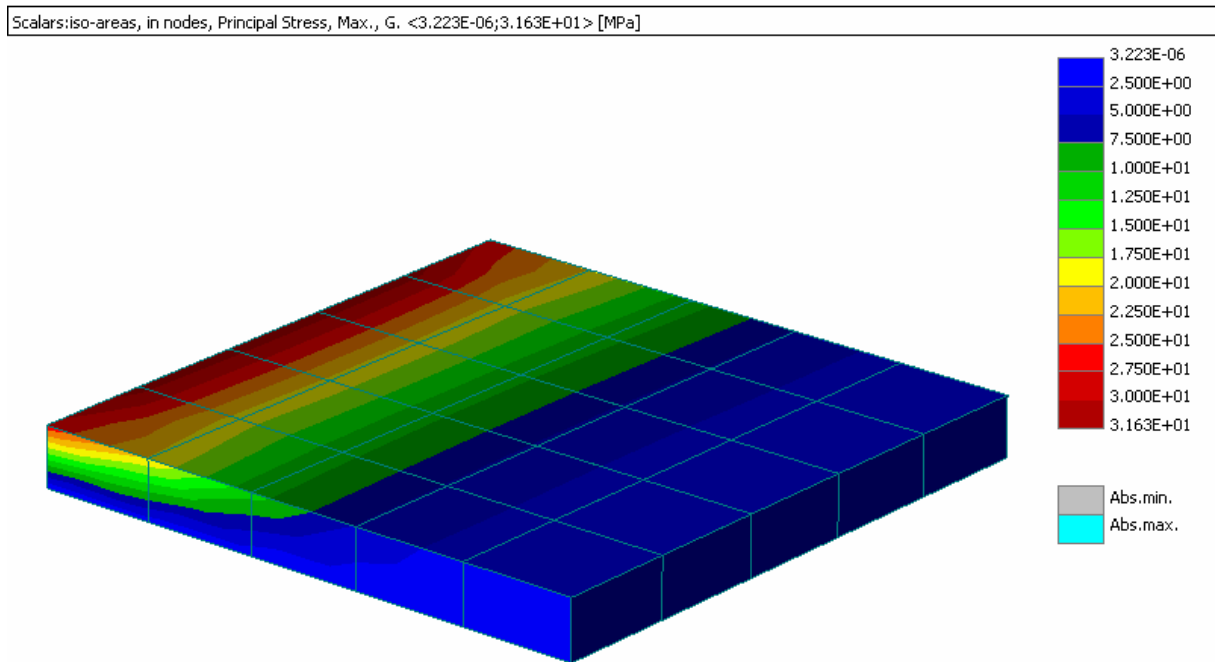


Figure 3-7 Shell elements. Mesh model with element size 0.2m, 10 layers. Iso-areas of axial stress (horizontal).

3.1.3 Conclusions

- (1) With sufficiently fine mesh all models give acceptable solution and agree well with the solution according to the Bernoulli beam hypothesis based on the assumption of plane section.
- (2) 2D plane stress element needs at least 4 elements through the thickness. One element through the thickness gives certainly wrong model. Although not shown in this study element aspect ratio (relation of width to height) is also important and should not be greater than 2.
- (3) Shell and 3D beam elements are far more efficient than 2D plane stress element in case of bending type of structure. The most important parameter is number of layers in shell, or fibers in beam. This is a similar feature as the number of integration points in solid elements. A recommended minimum number of layers is 4.
- (4) The study covers the range of elastic structure with mainly bending behavior, such as a cantilever beam. However, it gives a general information about efficiency of different elements. In case of nonlinear effects, such as plasticity and fracture, the mesh size effect may have different characteristics. The minimum number of elements holds also for nonlinear analysis.